Signal Processing 149 (2018) 14–26

Contents lists available at ScienceDirect

Signal Processing

journal homepage: www.elsevier.com/locate/sigpro

Efficient DOA estimation of noncircular signals in the presence of multipath propagation

Yuexian Wang*, Matthew Trinkle, Brian W.-H. Ng

University of Adelaide Radar Research Centre, School of Electrical and Electronic Engineering, The University of Adelaide, Adelaide, SA 5005, Australia

ARTICLE INFO

Article history:
Received 13 November 2016
Revised 18 February 2018
Accepted 5 March 2018
Available online 7 March 2018

Keywords:
Direction of arrival (DOA)
Noncircular signals
Coherent signals
Spatial smoothing

ABSTRACT

The noncircularity of uncorrelated signals can improve the performance of direction of arrival (DOA) estimation using antenna arrays. However, due to reflection from surfaces or malicious jamming, the received noncircular signals may be a mixture of uncorrelated and coherent components in practice, which has not been considered by existing algorithms. This paper addresses the issue of DOA estimation for noncircular signals under multipath fading in smart antenna systems, and a novel two-stage processing method is proposed accordingly. By expanding the signal subspace from augmented array output, the DOA estimates of uncorrelated sources are first obtained, and then the covariance matrix of uncorrelated signals is reconstructed and removed from that of the mixed signals afterwards. Secondly, a spatial smoothing technique is performed on a denoised covariance to restore rank deficiency in the covariance of the remaining coherent signals. The resultant algorithm can resolve more signals than array elements with higher accuracy and better classification of signal type than previous methods. Additionally, a new deterministic direction estimation Cramér–Rao lower bound (CRLB) is derived for the considered mixture model. Simulation results demonstrate the validity and efficiency of the proposed method.

1. Introduction

Direction of arrival (DOA) estimation for noncircular signals, which are omnipresent in radar, wireless communications, and satellite systems such as amplitude modulation (AM), binary phase shift keying (BPSK), amplitude shift keying (ASK), offset quadrature phase shift keying (OQPSK), and pulse amplitude modulation (PAM) signals, has been drawing increasing attention. The previous literature has shown that joint exploitation of the noncircularity of the incident signals helps to improve the performance of general DOA estimation methods [1–7]. Chargé et al.proposed the method of NC-Root-MUSIC (NC: noncircular) and showed that it has distinct advantages over the standard Root-MUSIC since it expands the effective array aperture and gives improvements both in the estimation accuracy and resolution [1]. For centro-symmetric arrays, the unitary ESPRIT algorithm was modified for noncircular signals increasing the number of resolvable signals and estimation accuracy in [2], and more recently *R*-dimensional ESPRIT-type algorithms have been developed and thoroughly analysed for this case [3]. Abeida and Delmas extensively investigated MUSIC-type algorithms for an arbitrary array geometry by providing closed-form expressions of the covariance of the asymptotic distribution of different projection matrices [4]. Combining high order cumulants and noncircularity, Liu et al. proposed NC-2*q*-MUSIC algorithm which is an extension of standard 2*q*-MUSIC to noncircular signals, further extending the effective array aperture and providing better performance compared with the original [5]. Gao et al.have addressed the DOA estimation and identification problems of simultaneous circular and noncircular signals in [6], while Chen et al. discussed the two-dimensional DOA estimation problem under the identical signal model [7]. Besides, some research work focuses on performance analysis of noncircular signal estimation algorithms in terms of the CRLB [8,9] and resolution [10]. However, the eigensystem-based algorithms reviewed above fail to work when uncorrelated and coherent signals coexist, as the spatial covariance matrix becomes rank deficient. This situation typically results from multipath propagation which is very common in urban areas.

To combat signal coherency, many rank recovery algorithms [11–15] have been proposed, among which forward/backward spatial smoothing (FBSS) [16] is commonly applied. However, FBSS does not fully utilise all the antenna elements because it resolves all the uncorrelated and coherent signals simultaneously. Processing the coherent and uncorrelated signals separately allows more sources than the number of array elements to be resolved. To

* Corresponding author.
E-mail addresses: yuexian.wang@hotmail.com, jwang@eleceng.adelaide.edu.au (Y. Wang), mtrinkle@eleceng.adelaide.edu.au (M. Trinkle), brian.ng@adelaide.edu.au (B.W.-H. Ng).

https://doi.org/10.1016/j.sigpro.2018.03.001
0165-1684/

achieve this, a pre-processing step that estimates and removes the uncorrelated signals, leaving only the coherent signals to be processed by FBSS is typically applied [17–22].

Rajagopal and Rao [17] initially conducted spatial differencing to separate coherent signals from the covariance matrix of received data, however, their algorithm could only resolve two sources in each coherent group. This work was followed up by Qi et al. [19] and Ye and Xu [20], who also used spatial differencing to separate the uncorrelated sources, and then introduced an additional processing step in the spatial smoothing algorithm to remove the extra spurious sources introduced by spatial differencing. Despite this, the additional processing step by Qi et al. lacks a theoretical proof and is just based on simulations, and it also does not completely recover all possible degrees of freedom. The method by Ye and Xu overcomes the limitations when only one coherent group exist, but helpless with multiple coherent groups case where it even resolve less signals than Qi's. Moreover, Ye's method has a high complexity and incurs a loss in DOA accuracy. In [21] the covariance matrix of coherent signals in [19] is replaced by a new constructed matrix which restores the number of resolvable coherent signals to the full number achievable without the spurious sources. This improves the DOA estimation accuracy and reduces the complexity. A new technique in [22] only uses a single subarray in the forward smoothing step which improves the accuracy but only allows pairs of coherent signals to be resolved. Additionally, two-stage processing technique has also been extended to fourth-order statistics (FOS) by [23] for non-Gaussian mixed signals and achieved satisfactory performance in unknown coloured Gaussian noise.

To the best of our knowledge, the previous literature has not considered coexistence of uncorrelated with coherent noncircular signals for DOA estimation. Different from the existing work, the approach proposed in this correspondence uses degree of freedom (DOF) in a more efficient manner and is particularly tailored to relax the constraint of the number of resolvable coherent noncircular signals. A subspace-based method is first applied to resolve the uncorrelated sources from the overall mixed signals. It exploits the characteristic of orthogonality between subspaces to classify the signal types. By reconstructing the covariance matrix of the uncorrelated noncircular sources, their contribution can be removed from the covariance matrix of the received data. Then, the spatial smoothing technique is applied to a denoised covariance matrix to resolve the remaining coherent signals. As we shall show in Section 3.3, the proposed method is capable of handling much more signals than sensors compared with the existing work on two-stage processing. In addition, we present the deterministic CRLBs for the noncircular signals in the considered multipath case. The CRLB was derived for the strict sense noncircular sources in [9]. However, it does not show the bound expression for noncircularity phase, nor is it applicable to coherent signals arising from multipath propagation. The derivation of CRLB in this paper can be viewed as a natural extension of the well-known results derived in [24,25] for the noncircular signal model.

The rest of the paper is organised as follows. In Section 2, the signal model when uncorrelated and coherent signals coexist is presented. In Section 3, we provide a two-stage preprocessing strategy to estimate the DOAs of the uncorrelated and coherent signals separately. In Section 4, simulation results show the validity and efficiency of our proposed method. Finally, some concluding remarks are given in Section 5.

Throughout this paper, the following notations will be used: the operators $(\cdot)^T$, $(\cdot)^*$, $(\cdot)^H$, $(\cdot)^{-1}$, $(\cdot)^+$, $E[\cdot]$, $\otimes$, $\odot$, and $\|\cdot\|_2$ denote the operation of transpose, conjugate, conjugate transpose, inverse, pseudo-inverse, expectation, Kronecker product, Schur-Hadamard product, and Euclidean (ℓ_2) norm, respectively. The complex operator j is defined by $j=\sqrt{-1}$. The notations $\mathrm{tr}\{\cdot\}$, $\mathrm{rank}(\cdot)$, $\mathrm{Re}\{\cdot\}$, and $\mathrm{Im}\{\cdot\}$ denote the trace operator, rank of a matrix, real part, and imaginary part of a complex number, respectively. The symbol $\mathrm{diag}\{z_1, z_2\}$ represents a diagonal matrix with diagonal entries z_1, z_2 and $\mathrm{blkdiag}\{\mathbf{Z}_1, \mathbf{Z}_2\}$ represents a block diagonal matrix with diagonal entries $\mathbf{Z}_1$, $\mathbf{Z}_2$. The symbol $\mathbf{Z}(a:b, c:d)$ denotes a submatrix constructed by the entries from a to bth row and c to dth column of $\mathbf{Z}$, and the symbol $\mathbf{Z}(a, b)$ denotes the entry in the ath row and bth column of $\mathbf{Z}$.

2. Problem formulation

2.1. Strictly second-order noncircular signals

For a noncircular signal $s(t)$, we have $E[s^2(t)] = \rho e^{j\phi} E[|s(t)|^2] = \rho e^{j\phi}\sigma_s^2$, where ϕ is the noncircularity phase and ρ is noncircularity rate which satisfies $0 < \rho \le 1$ (from the Cauchy–Schwartz inequality) [6,9]. A particular class of signals with $\rho = 1$, called strictly second-order (SO) noncircular signals, like AM, BPSK, OQPSK, and PAM signals, is widely used in radio communications [2,6,26]. In this case, the strictly SO noncircular signal can be expressed as $s(t) = e^{j\frac{\phi}{2}} s_0(t)$, where $\frac{\phi}{2}$ and $s_0(t)$ are the complex phase shift and real-valued symbol of $s(t)$, respectively. In this correspondence, we assume that all signals are strictly SO noncircular.

2.2. Array model for noncircular signals

Consider a number of N narrowband noncircular signals impinging on a uniform linear array (ULA) with M identical omnidirectional sensors. Assume that there are K groups of coherent signals, which come from K statistically independent far-field sources $s_k(t)$ with power σ_k^2 for $k = 1, 2, \ldots, K$, and with P_k multipath signals for each source. In the kth coherent group, the signal coming from direction θ_{kp}, $p = 1, 2, \ldots, P_k$ corresponds to the pth multipath propagation of the source $s_k(t)$, and the complex fading coefficient is α_{kp}. Denote the total number of coherent signals as $N_c = \sum_{k=1}^{K} P_k$, and assume the remaining $N_u = N - N_c$ sources $s_k(t)$ coming from direction θ_k with power σ_k^2, $k = N_c+1, N_c+2, \ldots, N$, are uncorrelated to each other and also to the coherent signals. The $M \times 1$ array output vector is then given by

$$\begin{aligned}\mathbf{x}(t) &= \sum_{k=1}^{K}\sum_{p=1}^{P_k} \mathbf{a}(\theta_{kp})\alpha_{kp} e^{j\frac{\phi_k}{2}} s_{k,0}(t) \\ &\quad + \sum_{k=N_c+1}^{N} \mathbf{a}(\theta_k) e^{j\frac{\phi_k}{2}} s_{k,0}(t) + \mathbf{n}(t) \\ &= \mathbf{A}_c \boldsymbol{\Gamma} \boldsymbol{\Psi}_c \mathbf{s}_{c,0}(t) + \mathbf{A}_u \boldsymbol{\Psi}_u \mathbf{s}_{u,0}(t) + \mathbf{n}(t) \\ &= \mathbf{A}\boldsymbol{\Upsilon}\boldsymbol{\Psi}\mathbf{s}_0(t) + \mathbf{n}(t) \end{aligned} \tag{1}$$

where $\mathbf{a}(\theta) = [1, e^{j\frac{2\pi d}{\lambda}\sin\theta}, \ldots, e^{j\frac{2\pi(M-1)d}{\lambda}\sin\theta}]^T \in \mathbb{C}^M$ is the steering vector with λ and d being the wavelength of carrier signal and the spacing between adjacent elements, respectively, $\mathbf{A}_c = [\mathbf{A}_{c,1}, \ldots, \mathbf{A}_{c,K}]$ with $\mathbf{A}_{c,k} = [\mathbf{a}(\theta_{k1}), \ldots, \mathbf{a}(\theta_{kP_k})]$, $\boldsymbol{\Gamma} = \mathrm{blkdiag}\{\boldsymbol{\alpha}_1, \ldots, \boldsymbol{\alpha}_K\}$ with $\boldsymbol{\alpha}_k = [\alpha_{k1}, \ldots, \alpha_{kP_k}]^T$ containing attenuation information of the kth coherent group, $\mathbf{A}_u = [\mathbf{a}(\theta_{N_c+1}), \mathbf{a}(\theta_{N_c+2}), \ldots, \mathbf{a}(\theta_N)]$, $\boldsymbol{\Psi}_c = \mathrm{diag}\{e^{j\frac{\phi_1}{2}}, e^{j\frac{\phi_2}{2}}, \ldots, e^{j\frac{\phi_K}{2}}\}$, $\boldsymbol{\Psi}_u = \mathrm{diag}\{e^{j\frac{\phi_{K+1}}{2}}, e^{j\frac{\phi_{K+2}}{2}}, \ldots, e^{j\frac{\phi_{K+N_u}}{2}}\}$, $\mathbf{s}_{c,0}(t) = [s_{1,0}(t), s_{2,0}(t), \ldots, s_{K,0}(t)]^T \in \mathbb{R}^K$, $\mathbf{s}_{u,0}(t) = [s_{K+1,0}(t), s_{K+2,0}(t), \ldots, s_{K+N_u}(t)]^T \in \mathbb{R}^{N_u}$, $\mathbf{A} = [\mathbf{A}_c, \mathbf{A}_u]$, $\boldsymbol{\Upsilon} = \mathrm{blkdiag}\{\boldsymbol{\Gamma}, \mathbf{I}\}$, $\boldsymbol{\Psi} = \mathrm{blkdiag}\{\boldsymbol{\Psi}_c, \boldsymbol{\Psi}_u\}$, $\mathbf{s}_0(t) = [\mathbf{s}_{c,0}^T(t), \mathbf{s}_{u,0}^T(t)]^T$, and $\mathbf{n}(t)$ is white Gaussian noise with the power σ_n^2 for each entry. Besides, we assume that the array is calibrated, and the array manifold $\mathbf{A}$ is unambiguous, i.e., the steering vectors $\{\mathbf{a}(\theta_i)\}_{i=1}^N$ are linearly independent for any set of distinct $\{\theta_i\}_{i=1}^N$. Equivalently, the matrix $\mathbf{A}$ is of full column rank.

In order to exploit the SO noncircularity of $\mathbf{x}(t)$ more conveniently, we construct an augmented observation vector

$$\begin{aligned}\tilde{\mathbf{x}}(t) &= \begin{bmatrix} \mathbf{J}\mathbf{x}^*(t) \\ \mathbf{x}(t) \end{bmatrix} \\ &= \begin{bmatrix} \mathbf{A}_c\boldsymbol{\Phi}_c^{1-M}\boldsymbol{\Gamma}^*\boldsymbol{\Psi}_c^* \\ \mathbf{A}_c\boldsymbol{\Gamma}\boldsymbol{\Psi}_c \end{bmatrix}\mathbf{s}_{c,0}(t) + \begin{bmatrix} \mathbf{A}_u\boldsymbol{\Phi}_u^{1-M}\boldsymbol{\Psi}_u^* \\ \mathbf{A}_u\boldsymbol{\Psi}_u \end{bmatrix}\mathbf{s}_{u,0}(t) \\ &\quad + \begin{bmatrix} \mathbf{J}\mathbf{n}^*(t) \\ \mathbf{n}(t) \end{bmatrix} \\ &= \tilde{\mathbf{A}}_c\mathbf{s}_{c,0}(t) + \tilde{\mathbf{A}}_u\mathbf{s}_{u,0}(t) + \tilde{\mathbf{n}}(t) \end{aligned} \tag{2}$$

where $\mathbf{J} \in \mathbb{R}^{M\times M}$ denotes an exchange matrix that has unity entries on the cross diagonal and zeros elsewhere, $\tilde{\mathbf{A}}_c = [(\mathbf{A}_c\boldsymbol{\Phi}_c^{1-M}\boldsymbol{\Gamma}^*\boldsymbol{\Psi}_c^*)^T, (\mathbf{A}_c\boldsymbol{\Gamma}\boldsymbol{\Psi}_c)^T]^T$, $\tilde{\mathbf{A}}_u = [(\mathbf{A}_u\boldsymbol{\Phi}_u^{1-M}\boldsymbol{\Psi}_u^*)^T, (\mathbf{A}_u\boldsymbol{\Psi}_u)^T]^T$, $\boldsymbol{\Phi}_c = \text{blkdiag}\{\boldsymbol{\Phi}_{c1}, \boldsymbol{\Phi}_{c2}, \ldots, \boldsymbol{\Phi}_{cK}\}$ with $\boldsymbol{\Phi}_{ck} = \text{diag}\{e^{j\frac{2\pi d}{\lambda}\sin\theta_{k1}}, e^{j\frac{2\pi d}{\lambda}\sin\theta_{k2}}, \ldots, e^{j\frac{2\pi d}{\lambda}\sin\theta_{kp_k}}\}$, $\boldsymbol{\Phi}_u = \text{diag}\{e^{j\frac{2\pi d}{\lambda}\sin\theta_{N_c+1}}, e^{j\frac{2\pi d}{\lambda}\sin\theta_{N_c+2}}, \ldots, e^{j\frac{2\pi d}{\lambda}\sin\theta_N}\}$, and $\tilde{\mathbf{n}}(t) = [(\mathbf{J}\mathbf{n}^*(t))^T, \mathbf{n}^T(t)]^T$.

The covariance matrix $\tilde{\mathbf{R}}$ of the newly constructed vector $\tilde{\mathbf{x}}(t)$ is then given by

$$\tilde{\mathbf{R}} = E[\tilde{\mathbf{x}}(t)\tilde{\mathbf{x}}^H(t)] = \tilde{\mathbf{A}}_c\mathbf{R}_c\tilde{\mathbf{A}}_c^H + \tilde{\mathbf{A}}_u\mathbf{R}_u\tilde{\mathbf{A}}_u^H + \sigma_n^2\mathbf{I}_{2M} \tag{3}$$

where $\mathbf{R}_c = E[\mathbf{s}_{c,0}(t)\mathbf{s}_{c,0}^H(t)] = \text{diag}\{\sigma_1^2, \sigma_2^2, \ldots, \sigma_K^2\}$, $\mathbf{R}_u = E[\mathbf{s}_{u,0}(t)\mathbf{s}_{u,0}^H(t)] = \text{diag}\{\sigma_{K+1}^2, \sigma_{K+2}^2, \ldots, \sigma_{K+N_u}^2\}$, and $\mathbf{I}$ represents a $2M\times 2M$ identity matrix. In the case of finite snapshots, the array covariance matrix can be calculated as $\hat{\mathbf{R}} = \frac{1}{L}\sum_{t=1}^{L}\tilde{\mathbf{x}}(t)\tilde{\mathbf{x}}^H(t)$, where L is the total number of snapshots.

3. DOA estimation

3.1. DOA estimation of the uncorrelated noncircular signals

When $K + N_u \le 2(M-1)$, the eigen-decomposition of $\tilde{\mathbf{R}}$ is given by

$$\tilde{\mathbf{R}} = \mathbf{U}\boldsymbol{\Sigma}\mathbf{U}^H = \mathbf{U}_s\boldsymbol{\Sigma}_s\mathbf{U}_s^H + \mathbf{U}_n\boldsymbol{\Sigma}_n\mathbf{U}_n^H \tag{4}$$

where $\boldsymbol{\Sigma} = \text{blkdiag}\{\boldsymbol{\Sigma}_s, \boldsymbol{\Sigma}_n\} = \text{diag}\{\lambda_1, \lambda_2, \ldots, \lambda_{2M}\}$ consists of $2M$ eigenvalues satisfying $\lambda_1 \ge \cdots \ge \lambda_{K+N_u} > \lambda_{K+N_u+1} = \cdots = \lambda_{2M}$. The columns of $\mathbf{U}_s \triangleq \mathbf{U}(:, 1:K+N_u)$ are the eigenvectors corresponding to the $K+N_u$ largest eigenvalues, while the columns of $\mathbf{U}_n \triangleq \mathbf{U}(:, K+N_u+1:M)$ are the eigenvectors corresponding to the rest $2M-K-N_u$ eigenvalues. Because the columns of $\mathbf{U}_s$ span the same signal subspace as that spanned by $[\tilde{\mathbf{A}}_c, \tilde{\mathbf{A}}_u]$, there is a nonsingular matrix $\mathbf{T} \in \mathbb{C}^{(K+N_u)\times(K+N_u)}$ that makes

$$\mathbf{U}_s = \begin{bmatrix} \tilde{\mathbf{A}}_c, \tilde{\mathbf{A}}_u \end{bmatrix}\mathbf{T}. \tag{5}$$

Let $\mathbf{J}_1 = \begin{bmatrix} \mathbf{I}_{M-1}, \mathbf{0}_{(M-1)\times 1} \end{bmatrix} \in \mathbb{R}^{(M-1)\times M}$ and $\mathbf{J}_2 = \begin{bmatrix} \mathbf{0}_{(M-1)\times 1}, \mathbf{I}_{M-1}, \end{bmatrix} \in \mathbb{R}^{(M-1)\times M}$. Here the signal subspace $\mathbf{U}_s$ can be divided into two matrices $\mathbf{U}_{s1} = (\mathbf{I}_2\otimes\mathbf{J}_1)\mathbf{U}_s$, $\mathbf{U}_{s2} = (\mathbf{I}_2\otimes\mathbf{J}_2)\mathbf{U}_s \in \mathbb{C}^{2(M-1)\times(K+N_u)}$. Evidently the structure in (5) is also valid for $\mathbf{U}_{s1}$ and $\mathbf{U}_{s2}$. If defining $\tilde{\mathbf{A}}_{c1} = (\mathbf{I}_2\otimes\mathbf{J}_1)\tilde{\mathbf{A}}_c$, $\tilde{\mathbf{A}}_{c2} = (\mathbf{I}_2\otimes\mathbf{J}_2)\tilde{\mathbf{A}}_c$, $\tilde{\mathbf{A}}_{u1} = (\mathbf{I}_2\otimes\mathbf{J}_1)\tilde{\mathbf{A}}_u$, $\tilde{\mathbf{A}}_{u2} = (\mathbf{I}_2\otimes\mathbf{J}_2)\tilde{\mathbf{A}}_u$, $\mathbf{A}_{c1} = \mathbf{J}_1\mathbf{A}_c$, $\tilde{\boldsymbol{\Gamma}}_c = \begin{bmatrix} \boldsymbol{\Phi}_c^{1-M}\boldsymbol{\Gamma}^*\boldsymbol{\Psi}_c^* \\ \boldsymbol{\Gamma}\boldsymbol{\Psi}_c \end{bmatrix}$, and $\tilde{\boldsymbol{\Phi}}_c = \mathbf{I}_2\otimes\boldsymbol{\Phi}_c$, and using $\tilde{\mathbf{A}}_c = (\mathbf{I}_2\otimes\mathbf{A}_c)\tilde{\boldsymbol{\Gamma}}_c$, one has $\tilde{\mathbf{A}}_{c1} = (\mathbf{I}_2\otimes\mathbf{J}_1)(\mathbf{I}_2\otimes\mathbf{A}_c)\tilde{\boldsymbol{\Gamma}}_c = (\mathbf{I}_2\otimes\mathbf{J}_1\mathbf{A}_c)\tilde{\boldsymbol{\Gamma}}_c = (\mathbf{I}_2\otimes\mathbf{A}_{c1})\tilde{\boldsymbol{\Gamma}}_c$. It is readily shown that $\mathbf{U}_{s1}^+ = \left(\begin{bmatrix} \tilde{\mathbf{A}}_{c1}, \tilde{\mathbf{A}}_{u1} \end{bmatrix}\mathbf{T}\right)^+ = \mathbf{T}^{-1}\begin{bmatrix} (\mathbf{I}_2\otimes\mathbf{A}_{c1})\tilde{\boldsymbol{\Gamma}}_c, \tilde{\mathbf{A}}_{u1} \end{bmatrix}^+$ as we have used the fact that $(\mathbf{BC})^+ = \mathbf{C}^+\mathbf{B}^+$ holds on condition that $\mathbf{B}$ is of full column rank and $\mathbf{C}$ is of full row rank and, hence

$$\mathbf{U}_{s1}^+\mathbf{U}_{s2} = \mathbf{T}^{-1}\begin{bmatrix} \mathbf{F}_1 & \mathbf{0}_{K\times N_u} \\ \mathbf{F}_2 & \boldsymbol{\Phi}_u \end{bmatrix}\mathbf{T} \tag{6}$$

where

$$\begin{bmatrix} \mathbf{F}_1 \\ \mathbf{F}_2 \end{bmatrix} = \begin{bmatrix} \tilde{\boldsymbol{\Gamma}}_c^H\left(\mathbf{I}_2\otimes\left(\mathbf{A}_{c1}^H\mathbf{A}_{c1}\right)\right)\tilde{\boldsymbol{\Gamma}}_c & \tilde{\boldsymbol{\Gamma}}_c^H\left(\mathbf{I}_2\otimes\mathbf{A}_{c1}^H\right)\tilde{\mathbf{A}}_{u1} \\ \tilde{\mathbf{A}}_{u1}^H(\mathbf{I}_2\otimes\mathbf{A}_{c1})\tilde{\boldsymbol{\Gamma}}_c & \tilde{\mathbf{A}}_{u1}^H\tilde{\mathbf{A}}_{u1} \end{bmatrix}^{-1} \times \begin{bmatrix} \tilde{\boldsymbol{\Gamma}}_c^H\left(\mathbf{I}_2\otimes\left(\mathbf{A}_{c1}^H\mathbf{A}_{c1}\right)\right)\tilde{\boldsymbol{\Phi}}_c\tilde{\boldsymbol{\Gamma}}_c \\ \tilde{\mathbf{A}}_{u1}^H(\mathbf{I}_2\otimes\mathbf{A}_{c1})\tilde{\boldsymbol{\Phi}}_c\tilde{\boldsymbol{\Gamma}}_c \end{bmatrix}. \tag{7}$$

The proof of (6) is given in Appendix A.

This result shows that $\mathbf{U}_{s1}^+\mathbf{U}_{s2}$ is *similar* to $\begin{bmatrix} \mathbf{F}_1 & \mathbf{0}_{K\times N_u} \\ \mathbf{F}_2 & \boldsymbol{\Phi}_u \end{bmatrix}$. Hence, the eigenvalues of these two matrices are identical to each other, and the N_u diagonal entries of $\boldsymbol{\Phi}_u$ are included in the nonzero eigenvalues of $\begin{bmatrix} \mathbf{F}_1 & \mathbf{0}_{K\times N_u} \\ \mathbf{F}_2 & \boldsymbol{\Phi}_u \end{bmatrix}$ (See Appendix B for proof). However, we can obtain the K eigenvalues associated with the K groups of the coherent noncircular signals in addition to the eigenvalues of the N_u uncorrelated noncircular signals. As a consequence, it is necessary to provide a robust criterion to identify the DOA of uncorrelated noncircular signals from the false ones.

Firstly, if the eigenvalues of $\mathbf{U}_{s1}^+\mathbf{U}_{s2}$ are denoted as $\{\eta_k\}_{k=1}^{K+N_u}$, then all DOA estimate candidates, $\hat{\theta}_k$, of uncorrelated noncircular signals can be obtained by

$$\hat{\theta}_k = \arcsin\left(\frac{\lambda}{2\pi d}\arg(\eta_k)\right), \quad k = 1, 2, \ldots, K+N_u. \tag{8}$$

Then, let us define a spatial spectrum function

$$f(\theta,\phi) \triangleq \tilde{\mathbf{a}}(\theta,\phi)^H\mathbf{U}_n\mathbf{U}_n^H\tilde{\mathbf{a}}(\theta,\phi) \tag{9}$$

where

$$\tilde{\mathbf{a}}(\theta,\phi) = \begin{bmatrix} \mathbf{a}(\theta)e^{j\frac{2\pi(1-M)d}{\lambda}\sin\theta}e^{-j\frac{\phi}{2}} \\ \mathbf{a}(\theta)e^{j\frac{\phi}{2}} \end{bmatrix}. \tag{10}$$

To separate parameterisation for noncircular phase and DOA, (10) can be rewritten as

$$\begin{aligned}\tilde{\mathbf{a}}(\theta,\phi) &= \begin{bmatrix} \mathbf{a}(\theta)e^{j\frac{2\pi(1-M)d}{\lambda}\sin\theta} & \\ & \mathbf{a}(\theta) \end{bmatrix}\begin{bmatrix} e^{-j\frac{\phi}{2}} \\ e^{j\frac{\phi}{2}} \end{bmatrix} \\ &= \mathbf{E}(\theta)\mathbf{c}(\phi) \end{aligned} \tag{11}$$

where $\mathbf{E}(\theta) \triangleq \text{blkdiag}\left\{\mathbf{a}(\theta)e^{j\frac{2\pi(1-M)d}{\lambda}\sin\theta}, \mathbf{a}(\theta)\right\} \in \mathbb{C}^{2M\times 2}$ and $\mathbf{c}(\phi) \triangleq \begin{bmatrix} e^{-j\frac{\phi}{2}}, e^{j\frac{\phi}{2}} \end{bmatrix}^T$. Then, substituting (11) into (9), one gets

$$f(\theta,\phi) = \mathbf{c}^H(\phi)\mathbf{M}(\theta)\mathbf{c}(\phi) \tag{12}$$

where

$$\mathbf{M}(\theta) = \mathbf{E}(\theta)^H\mathbf{U}_n\mathbf{U}_n^H\mathbf{E}(\theta). \tag{13}$$

We now show how to verify the true DOA estimates of uncorrelated signals based on the determinant or the smallest eigenvalue of $\mathbf{M}(\theta)$. It can be found that the dimension of $\mathbf{E}(\theta)^H\mathbf{U}_n$ is $2\times(2M-K-N_u)$. Because of the condition $K+N_u \le 2(M-1)$, i.e., $2 \le (2M-K-N_u)$, the matrix $\mathbf{E}(\theta)^H\mathbf{U}_n$, in general, is full row rank and $\mathbf{M}(\theta)$ is full rank. However, due to the orthogonality between the signal subspace spanned by $\tilde{\mathbf{A}}_u$ and the noise subspace spanned by $\mathbf{U}_n$, when θ coincides with any one of the N_u desired DOAs of uncorrelated signals, i.e., $\theta = \theta_k$ ($k = K+1, K+2, \ldots, K+N_u$), the function $f(\theta, \phi)$ in (12) becomes zero. Since $\mathbf{c} \neq \mathbf{0}$, (12) can hold true only if the matrix $\mathbf{M}(\theta)$ is rank deficient or, equivalently, its determinant (as well as its smallest eigenvalue) is equal to zero [27,28]. This orthogonality no longer holds for coherent signals, consequently, the determinant of $\mathbf{M}(\theta)$ can be utilised to verify the true DOA estimates. In the finite snapshots case, the true DOA estimates of the N_u uncorrelated signals correspond to the minima of

the verification equation $\det\left\{\mathbf{M}(\hat{\theta})\right\}$ which remains large for the remaining K false estimates. In this way, the true estimates can be selected and the false ones can be effectively eliminated.

The noncircularity phases of the uncorrelated signals are subsequently given by the minima of (9). By partitioning $\mathbf{U}_n$ into the two submatrices with the same dimension $\mathbf{U}_{n1} = \mathbf{U}_n(1:M,:)$, $\mathbf{U}_{n2} = \mathbf{U}_n(M+1:2M,:)$, and setting the partial derivative of (9) to zero, i.e., $\frac{\partial f(\theta,\phi)}{\partial \theta} = 0$, we find that when

$$e^{j\phi} = -\frac{\mathbf{a}^H(\theta)\mathbf{U}_{n2}\mathbf{U}_{n1}^H\mathbf{a}(\theta)e^{j\frac{2\pi(1-M)d}{\lambda}\sin\theta}}{\left|\mathbf{a}^H(\theta)\mathbf{U}_{n2}\mathbf{U}_{n1}^H\mathbf{a}(\theta)e^{j\frac{2\pi(1-M)d}{\lambda}\sin\theta}\right|}, \tag{14}$$

(9) will achieve its minima. Once the true DOA estimates of uncorrelated signals are obtained, the corresponding noncircularity phases will be estimated accordingly.

3.2. DOA estimation of the coherent noncircular signals

Next we will deal with the coherent noncircular signals. The coherent signal DOAs are estimated by first removing the uncorrelated signals from the covariance matrix $\tilde{\mathbf{R}}$ and then resolving the coherent signals by performing spatial smoothing on the eigenvectors of the resulting covariance matrix for rank restoration. In this way, the proposed method separates the two types of signals and provides improved estimation accuracy.

After obtaining the DOA and noncircularity phase estimates of the uncorrelated signals, one can construct the following vector

$$\mathbf{b}(\theta,\phi) = \begin{bmatrix} \mathbf{a}(\theta)e^{j\frac{2\pi(1-M)d}{\lambda}\sin\theta} \\ \mathbf{a}(\theta)e^{j\phi} \end{bmatrix} = e^{j\frac{\phi}{2}}\tilde{\mathbf{a}}(\theta,\phi) \tag{15}$$

which has the same subspace as $\tilde{\mathbf{a}}(\theta,\phi)$. Then the power of the uncorrelated signals can be estimated by

$$\sigma_k^2 = \frac{1}{\mathbf{b}^H(\theta_k,\phi_k)\left(\tilde{\mathbf{R}} - \sigma_n^2\mathbf{I}\right)^+\mathbf{b}(\theta_k,\phi_k)} \tag{16}$$

where σ_n^2 can be estimated as the mean of the $2M-K-N_u$ smallest eigenvalues of $\tilde{\mathbf{R}}$. The proof of (16) is provided in Appendix C.

From (16), we define $\mathbf{R}_{su} \triangleq \mathrm{diag}\{\sigma_{K+1}^2,\ldots,\sigma_{K+N_u}^2\}$ and $\mathbf{B}_u \triangleq [\mathbf{b}(\theta_{K+1},\phi_{K+1}),\ldots,\mathbf{b}(\theta_{K+N_u},\phi_{K+N_u})] = \tilde{\mathbf{A}}_u\boldsymbol{\Psi}_{\boldsymbol{u}}$. Given $\mathbf{B}_u$ and $\mathbf{R}_{su}$, we can form a matrix $\mathbf{R}_{xc}$ as

$$\begin{aligned}\mathbf{R}_{xc} &\triangleq \tilde{\mathbf{R}} - \mathbf{B}_u\mathbf{R}_{su}\mathbf{B}_u^H - \sigma_n^2\mathbf{I} \\ &= \tilde{\mathbf{R}} - \tilde{\mathbf{A}}_u\boldsymbol{\Psi}_u\mathbf{R}_{su}\boldsymbol{\Psi}_u^H\tilde{\mathbf{A}}_u^H - \sigma_n^2\mathbf{I} \\ &= \tilde{\mathbf{R}} - \tilde{\mathbf{A}}_u\mathbf{R}_{su}\tilde{\mathbf{A}}_u^H - \sigma_n^2\mathbf{I} \\ &= \tilde{\mathbf{A}}_c\mathbf{R}_c\tilde{\mathbf{A}}_c^H.\end{aligned} \tag{17}$$

Clearly, $\mathbf{R}_{xc}$ only contains the information of coherent signals.

After removing the uncorrelated source components from $\tilde{\mathbf{R}}$, the rank of the remaining coherent signals in $\mathbf{R}_{xc}$ is restored using a spatial smoothing technique.

Performing the eigen-decomposition of $\mathbf{R}_{xc}$, we have

$$\mathbf{R}_{xc} = \mathbf{U}_{cs}\boldsymbol{\Sigma}_{cs}\mathbf{U}_{cs}^H + \mathbf{U}_{cn}\boldsymbol{\Sigma}_{cn}\mathbf{U}_{cn}^H \tag{18}$$

where $\mathbf{U}_{cs} \in \mathbb{C}^{2M\times K}$ is a matrix whose columns are the eigenvectors corresponding to the K largest eigenvalues, and $\mathbf{U}_{cn} \in \mathbb{C}^{2M\times(2M-K)}$ spans the noise subspace associated with the remaining $2M-K$ smallest eigenvalues which are contained in $\boldsymbol{\Sigma}_{cn}$. As the noise components have been eliminated in (17), ideally, $\boldsymbol{\Sigma}_{cn}$ is supposed to be $\mathbf{0}_{(2M-K)\times(2M-K)}$. However, due to the estimation errors of DOA, noncircularity phase, and signal power, $\boldsymbol{\Sigma}_{cn}$ will not go to zero in practice.

In order to mitigate the noise effect, denoising will be applied before the smoothing step, which would correspond to smoothing on $\mathbf{U}_{cs}\boldsymbol{\Sigma}_{cs}\mathbf{U}_{cs}^H$ (i.e., truncating the small, noise-related eigenvalues of $\mathbf{R}_{xc}$). Let us define $\bar{\mathbf{J}}_r = \left[\mathbf{0}_{m\times(r-1)}, \mathbf{I}_m, \mathbf{0}_{m\times(q-r)}\right] \in \mathbb{R}^{m\times M}$, which selects m out of M rows, indexed by r. Here, we divide $\mathbf{U}_{cs}\boldsymbol{\Sigma}_{cs}\mathbf{U}_{cs}^H$ into multiple $2m\times 2m$ submatrices as

$$\mathbf{R}_r^f = \left(\mathbf{I}_2\otimes\bar{\mathbf{J}}_r\right)\mathbf{U}_{cs}\boldsymbol{\Sigma}_{cs}\mathbf{U}_{cs}^H\left(\mathbf{I}_2\otimes\bar{\mathbf{J}}_r\right)^H \tag{19}$$

and then $q = M-m+1$ submatrices become available. The spatial smoothed covariance matrix is given by

$$\begin{aligned}\mathbf{R}_{ss} &= \frac{1}{q}\sum_{r=1}^{q}\left(\mathbf{I}_2\otimes\bar{\mathbf{J}}_r\right)\mathbf{U}_{cs}\boldsymbol{\Sigma}_{cs}\mathbf{U}_{cs}^H\left(\mathbf{I}_2\otimes\bar{\mathbf{J}}_r\right)^H \\ &= \frac{1}{q}\sum_{r=1}^{q}\left(\mathbf{I}_2\otimes\bar{\mathbf{J}}_r\right)\mathbf{U}_{cs}\boldsymbol{\Sigma}_{cs}\mathbf{U}_{cs}^H\left(\mathbf{I}_2\otimes\bar{\mathbf{J}}_r^T\right)\end{aligned} \tag{20}$$

where $\mathbf{U}_{cs} = [\mathbf{u}_1,\mathbf{u}_2,\ldots,\mathbf{u}_K]$. Since $\mathbf{U}_{cs} = \tilde{\mathbf{A}}_c\mathbf{T}$, inserting it into (20) gives

$$\begin{aligned}\mathbf{R}_{ss} &= \frac{1}{q}\sum_{r=1}^{q}\left(\mathbf{I}_2\otimes\bar{\mathbf{J}}_r\right)\tilde{\mathbf{A}}_c\mathbf{T}\boldsymbol{\Sigma}_{cs}\mathbf{T}^H\tilde{\mathbf{A}}_c^H\left(\mathbf{I}_2\otimes\bar{\mathbf{J}}_r^T\right) \\ &= \frac{1}{q}\sum_{r=1}^{q}\left(\mathbf{I}_2\otimes\bar{\mathbf{J}}_r\right)\tilde{\mathbf{A}}_c\tilde{\mathbf{T}}\tilde{\mathbf{T}}^H\tilde{\mathbf{A}}_c^H\left(\mathbf{I}_2\otimes\bar{\mathbf{J}}_r^T\right)\end{aligned} \tag{21}$$

where $\tilde{\mathbf{T}} = \mathbf{T}\boldsymbol{\Sigma}_{cs}^{\frac{1}{2}}$.

Next we examine whether the rank of $\mathbf{R}_{ss}$ has been restored sufficiently to resolve N_c coherent noncircular signals.

Proposition 1. *When* $2m \geq N_c+1$ *and* $q \geq P_{\max}$, $\mathrm{rank}(\mathbf{R}_{ss}) = N_c$ *for* K *groups of coherent noncircular signals, where* $P_{\max} = \max\{P_1,P_2,\ldots,P_K\}$.

The proof of Proposition 1 is given in Appendix D.

One can subsequently follow prevailing subspace methods, such as MUSIC [29] or ESPRIT [30], to resolve the DOA estimates of the coherent signals.

As the spatial smoothing operation renders a reduced array aperture and DOFs, the estimation accuracy is still confined even though the noise elements have been alleviated. However, once the coarse DOA estimates are obtained, one can identify and group the paths associated with the same source together, then the refined DOA estimates can be determined by a spectral rank reduction (RARE) estimator that allows an enhanced effective aperture, and better performance can thus be expected.

Given the coarse DOA estimates, one can associate all paths with different sources by examining dependency between different signal components, as suggested in [31]. To be more specific, from the coarse DOA estimates of coherent signals, one can reconstruct $\mathbf{A}_c$ and find $2K$ eigenvectors $\tilde{\mathbf{q}}_k$, $k=1,2,\ldots,2K$, corresponding to the $2K$ minimum eigenvalues of $\tilde{\mathbf{P}} = \begin{bmatrix}\mathbf{J}\mathbf{A}_c^* \\ \mathbf{A}_c\end{bmatrix}^H\mathbf{U}_{cn}\mathbf{U}_{cn}^H\begin{bmatrix}\mathbf{J}\mathbf{A}_c^* \\ \mathbf{A}_c\end{bmatrix}$, then divide rows of $\tilde{\mathbf{Q}} = [\tilde{\mathbf{q}}_1,\tilde{\mathbf{q}}_2,\ldots,\tilde{\mathbf{q}}_{2K}]$ into K groups, where the rows in the same group are dependent of each other, while the rows in different groups are independent of each other. These K groups of rows correspond to the K groups of paths associated with the K sources. Since the columns of $\tilde{\mathbf{A}}_c$ span the signal subspace, which coincides with the column space of $\mathbf{U}_{cs}$, and the signal subspace is orthogonal to the noise subspace spanned by the columns of $\mathbf{U}_{cn}$, one has

$$\begin{aligned}&\left\|\begin{bmatrix}e^{-j\frac{\phi_k}{2}}\mathbf{J}\mathbf{A}_{c,k}^*\boldsymbol{\alpha}_k^* \\ e^{j\frac{\phi_k}{2}}\mathbf{A}_{c,k}\boldsymbol{\alpha}_k\end{bmatrix}^H\mathbf{U}_{cn}\right\|_2^2 = \left\|\left(\tilde{\mathbf{E}}_k\tilde{\boldsymbol{\alpha}}_k\right)^H\mathbf{U}_{cn}\right\|_2^2 \\ &= \tilde{\boldsymbol{\alpha}}_k^H\tilde{\mathbf{E}}_k^H\mathbf{U}_{cn}\mathbf{U}_{cn}^H\tilde{\mathbf{E}}_k\tilde{\boldsymbol{\alpha}}_k \\ &= \tilde{\boldsymbol{\alpha}}_k^H\tilde{\mathbf{M}}_k\tilde{\boldsymbol{\alpha}}_k = 0\end{aligned} \tag{22}$$

Table 1
Summary of the two-stage processing method.

Step 1.	Construct the augmented observation vector $\tilde{\mathbf{x}}(t) \in \mathbb{C}^{2M}$ according to (2) and then compute the covariance matrix $\hat{\mathbf{R}} = \frac{1}{L}\sum_{t=1}^{L} \tilde{\mathbf{x}}(t)\tilde{\mathbf{x}}^H(t)$.
Step 2.	DOA estimation of uncorrelated noncircular signals: • Calculate $\mathbf{U}_s$ from the eigen-decomposition of $\hat{\mathbf{R}}$, and divide it into two matrices $\mathbf{U}_{s1} = (\mathbf{I}_2 \otimes \mathbf{J}_1)\mathbf{U}_s$ and $\mathbf{U}_{s2} = (\mathbf{I}_2 \otimes \mathbf{J}_2)\mathbf{U}_s \in \mathbb{C}^{2(M-1)\times(K+N_u)}$. • Obtain the eigenvalues of $\mathbf{U}_{s1}^{+}\mathbf{U}_{s2}$ and determine the DOA estimate candidates in (8). • Sift the true DOA estimates of uncorrelated signals by finding N_u minima of $\det\left\{\mathbf{M}(\hat{\theta})\right\}$.
Step 3.	Extraction of covariance matrix of coherent signals: • Estimate the noncircularity phases of uncorrelated signals according to (14). • Estimate the power of uncorrelated signals in (16). • Extract $\mathbf{R}_{xc}$ from $\hat{\mathbf{R}}$ in (17).
Step 4.	Coarse DOA estimation of coherent noncircular signals: • Calculate $\mathbf{U}_{cs}\mathbf{\Sigma}_{cs}\mathbf{U}_{cs}^H$ from the eigen-decomposition of $\mathbf{R}_{xc}$ and then get the smoothed matrix $\mathbf{R}_{ss}$ in (20). • Determine the coarse DOA estimates of coherent signals by using ordinary MUSIC or ESPRIT.
Step 5.	DOA estimation refinement of coherent signals: • Reconstruct $\mathbf{A}_c$ and find $2K$ eigenvectors $\tilde{\mathbf{q}}_k$ corresponding to the $2K$ minimum eigenvalues of $\tilde{\mathbf{P}}$. • Divide rows of $\tilde{\mathbf{Q}}$ into K groups and associate all paths with different sources. • Refine DOA estimates by searching the minimum of $\det\left\{\tilde{\mathbf{M}}_k\right\}$.

where $\tilde{\mathbf{E}}_k \triangleq \text{blkdiag}\left\{\mathbf{J}\mathbf{A}_{c,k}^{*}, \mathbf{A}_{c,k}\right\}$, $\tilde{\boldsymbol{\alpha}}_k \triangleq \left[e^{-j\frac{\phi_k}{2}}\boldsymbol{\alpha}_k^H, e^{j\frac{\phi_k}{2}}\boldsymbol{\alpha}_k^T\right]^T$, and $\tilde{\mathbf{M}}_k = \tilde{\mathbf{E}}_k^H\mathbf{U}_{cn}\mathbf{U}_{cn}^H\tilde{\mathbf{E}}_k$. As $\tilde{\boldsymbol{\alpha}}_k \neq \mathbf{0}$, (22) can hold true only if $\tilde{\mathbf{M}}_k$ is rank deficient or, equivalently, its determinant is equal to zero. Since the coarse DOA estimates have been provided, DOA estimation refinement can be performed by searching the minimum of $\det\left\{\tilde{\mathbf{M}}_k\right\}$ for the kth coherent group in a small subset of the space $\mathbf{\Omega}_k$ that is defined by

$$\mathbf{\Omega}_k = \boldsymbol{\theta}_{k1} \cup \boldsymbol{\theta}_{k2} \cup \cdots \boldsymbol{\theta}_{kP_k} \tag{23}$$

where $\boldsymbol{\theta}_{ki} = \left[\hat{\theta}_{ki} - \delta_{ki}, \hat{\theta}_{ki} + \delta_{ki}\right]$, $\hat{\theta}_{ki}$ is the ith coarse DOA estimate of the kth coherent group and δ_{ki} controls the size of the search space around $\hat{\theta}_{ki}$. It is worth noting that the above method acts as a coarse-to-fine procedure, therefore, δ_{ki} can be small in general. In fact, the refinement technique bears some resemblance to the RARE estimator in [27,28] as the rank reduction property is tailored herein to fit the noncircular case. Compared with the signal subspace of the rth submatrix in spatial smoothing $\left(\mathbf{I}_2 \otimes \tilde{\mathbf{J}}_r\right)\mathbf{U}_{cs} \in \mathbb{C}^{2m\times K}$, $\tilde{\mathbf{E}}_k \in \mathbb{C}^{2M\times 2P_k}$ in (22) has a larger array aperture and DOFs, which implies that estimation performance of coherent signals can be further improved. The major steps of the proposed algorithm are summarised in Table 1.

Remark 1. In the process of refining DOA estimates, the main complexity attributes to the multidimensional grid search, which is often computationally expensive. In order to facilitate the analysis, we assume that the number of sampling grids for each $\boldsymbol{\theta}_{ki}$ is G. The resultant flops involved in the refinement are $\mathcal{O}\left(8\sum_{k=1}^{K} G^{P_k}P_k^3\right)$. Here, a flop stands for a complex-valued floating point multiplication operation. It can be seen that if P_k is relatively small, the computation consumption is affordable.

Remark 2. For the partially correlated sources, however, the case may be different. When the sources are mildly correlated, say the correlation coefficient $\eta = 0.2$, the estimation by the method of Section 3.1 is better than that obtained from Section 3.2. This is because most of the power of the mildly correlated signals is estimated and then subtracted from the covariance matrix of the observations. By contrast, when the sources are highly correlated, say $\eta = 0.8$, the estimation in Section 3.2 may be more accurate than that in Section 3.1, especially at low SNRs. The reason is that most of the power of highly correlated signals has to be maintained, although the array aperture is reduced to relieve the coherency. When the sources are moderately correlated, say $\eta = 0.5$, it is necessary to estimate a non-diagonal source covariance matrix, however, we are not able to perform such step as the structure of source covariance matrix is generally arbitrary and difficult to be modelled. The discussion on the case of partially correlated sources can also be found in [21]. The partially correlated source case is particularly relevant in the sample-starved scenario. The reason is that even if sources are (statistically) uncorrelated, the sample correlation we observe from a small number of snapshots may be significant, which implies that the proposed scheme requires a (couple of) hundred snapshots to show satisfactory performance.

3.3. Identifiability of DOA estimation

This section discusses the maximum number of separable signals by the proposed scheme. The uncorrelated and coherent noncircular signals are resolved separately, which makes best use of the DOF of the original ULA and allows more signals than sensors ($N \geq M$) to be estimated. Compared with the standard FBSS, which estimates the uncorrelated and coherent signals simultaneously, and spatial difference smoothing method in [19], referred to as SDS, which cannot extend effective aperture for uncorrelated signals, the maximum number of signals estimated by our method can be increased beyond the traditional limit. If $2(M-1) \geq K + N_u$, $2m > N_c$, and $q \geq P_{\max}$, we can estimate a maximum number of $2M - K - 2$ uncorrelated noncircular sources plus $2(M - P_{\max})$ coherent noncircular signals since $M \geq \lceil \frac{N_c}{2} \rceil + P_{\max}$, while the FBSS can estimate at most $M - \lceil \frac{P_{\max}}{2} \rceil$ mixed signals, and SDS can achieve the upper bound of $M - K - 1$ uncorrelated signals plus $M - \lceil \frac{P_{\max}}{2} \rceil$ coherent signals on condition that $M - 1 \geq K + N_u$, $m > N_c$ and $2q \geq P_{\max}$, where $\lceil \cdot \rceil$ is the ceiling operator. Although in general spatial differencing methods for separating the coherent signals from uncorrelated sources can also process more signals than array sensors, they ignore the noncircularity of the incident signals, and thus can not improve the DOF for uncorrelated noncircular signal estimation. Besides, spatial differencing will eliminate part of the coherent signal information (i.e., the entries along the cross diagonal of the covariance matrix of $\mathbf{x}(t)$) in addition to the uncorrelated signal components. Thirdly, extra processing proce-

Table 2
Minimum number of array elements required.

Uncorr-elated signals	Coherent signals		Total sign-als	Number of array elements			
	Groups	Signals in each group		FBSS	SDS	RSDS	PROP-OSED
2	1	2	4	5	5	4	3
2	2	2	6	7	6	5	4
4	1	4	8	10	7	6	6
4	2	2	8	9	8	7	4
3	3	2	9	10	8	7	6
5	2	3	11	13	9	8	5
5	3	2	11	12	10	9	6
6	3	3	15	17	12	11	8

dures are required to identify and alleviate pseudo-DOA estimates which are also caused by the differencing operation [19]. A rectified spatial differencing technique [21], referred to as RSDS, can achieve one more DOF for resolving coherent signals than SDS after rank restoration, but it is less accurate.

Table 2 lists the minimum number of array elements required to resolve a given number of signals by the four methods. For simplicity, we assume that each group has the same number of coherent signals. We can see that our method can use fewer array elements than any other algorithms to estimate the same number of signals.

4. Simulation results and discussion

In this section, a series of numerical experiments under different conditions are conducted to examine the performance of the proposed method. Simulations are carried out for a ten-element ULA with half-wavelength spacing between adjacent elements. For simplicity, we assume that all noncircular signals are BPSK modulated with the same symbol duration, and these BPSK signals, uncorrelated and coherent, have identical power σ_s^2, and the input SNR is defined as $10\log_{10}(\sigma_s^2/\sigma_n^2)$. RSDS, SDS, and FBSS are chosen for comparison. The accuracy of the estimates is measured from 1000 Monte Carlo runs in terms of the root mean square error (RMSE) which is defined as

$$\mathrm{RMSE}_\theta = \sqrt{\frac{1}{1000I}\sum_{n=1}^{1000}\sum_{i=1}^{I}(\hat{\theta}_i^{(n)}-\theta_i)^2} \tag{24}$$

$$\mathrm{RMSE}_\phi = \sqrt{\frac{1}{1000J}\sum_{n=1}^{1000}\sum_{j=1}^{J}(\hat{\phi}_j^{(n)}-\phi_j)^2} \tag{25}$$

where $\hat{\theta}_i^{(n)}$ is the estimate of θ_i for the nth trial, I is the number of all uncorrelated or coherent signals, and J is the number of noncircularity phases of the uncorrelated signals. Note that here we use different indices i for the signals, since they are estimated at different stages. In (23), δ_{ki} is chosen to be $\delta_{k1}=\delta_{k2}=\cdots=\delta_{kP_k}=2^\circ$.

4.1. DOA estimation of coherent signals only

To assess the performance of the four algorithms on DOA estimation of coherent signals, we assume that there are two groups of two coherent signals from $[-41^\circ,-21^\circ]$ and $[5^\circ, 20^\circ]$ impinging on the ULA. The fading coefficients of the coherent signals are $[-0.0054-j,-0.6889-0.1241j]$ and $[0.7568-0.6537j, 0.7202+0.3483j]$, respectively. The noncircularity phases are $[129.56^\circ, 205.78^\circ]$. We select $m=3$ in this scenario.

The resultant RMSE versus SNR for 200 snapshots and RMSE versus the number of snapshots for SNR $=-5$ dB are compared in Fig. 1. It is noticed that the noncircular refinement method outperforms its circular counterpart as the former exploits the extra noncircular information while the latter takes the circular information only. Besides, both proposed refinement methods, circular and noncircular, offer much better performance than FBSS and RSDS. As a matter of fact, the superiority of the proposed spatial smoothing with refinement becomes more considerable when the size of submatrix in spatial smoothing operation tends to be smaller, i.e., smoothing the rank deficient matrix excessively. It is also found from Fig. 1 that the proposed spatial smoothing method without refinement, FBSS, and RSDS achieve approximately the same performance at mildly high SNRs if only coherent signals arise.

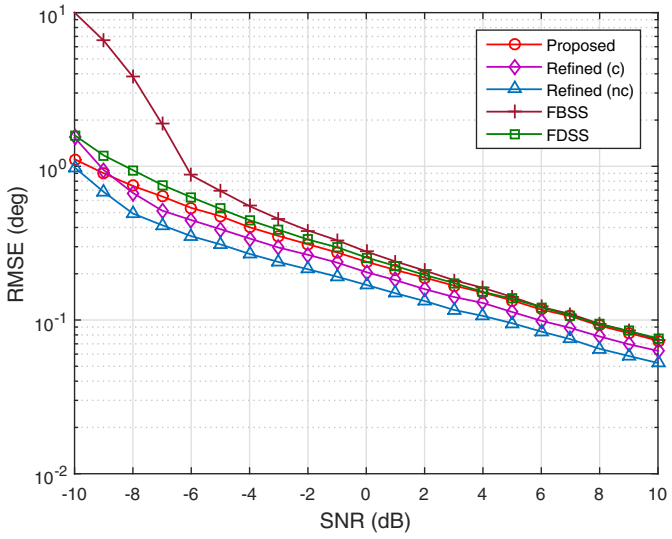

(a)

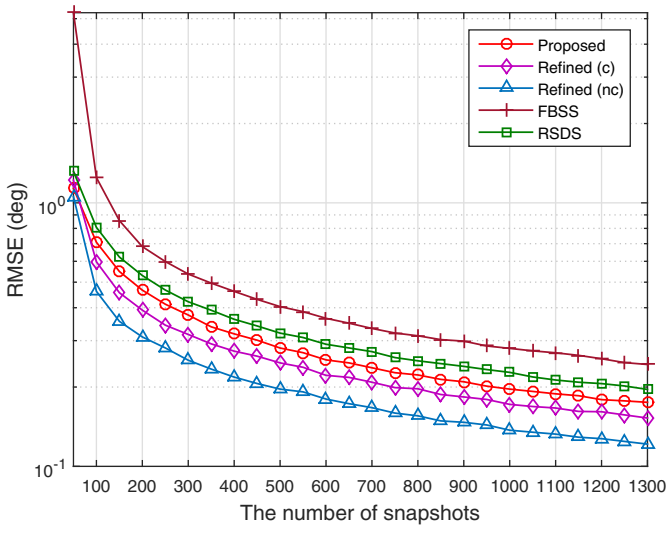

(b)

Fig. 1. RMSE of the coherent signal estimates versus (a) SNR when the number of snapshots is 200; (b) the number of snapshots when SNR $=-5$ dB for the noncircular "(nc)" source and the circular "(c)" source.

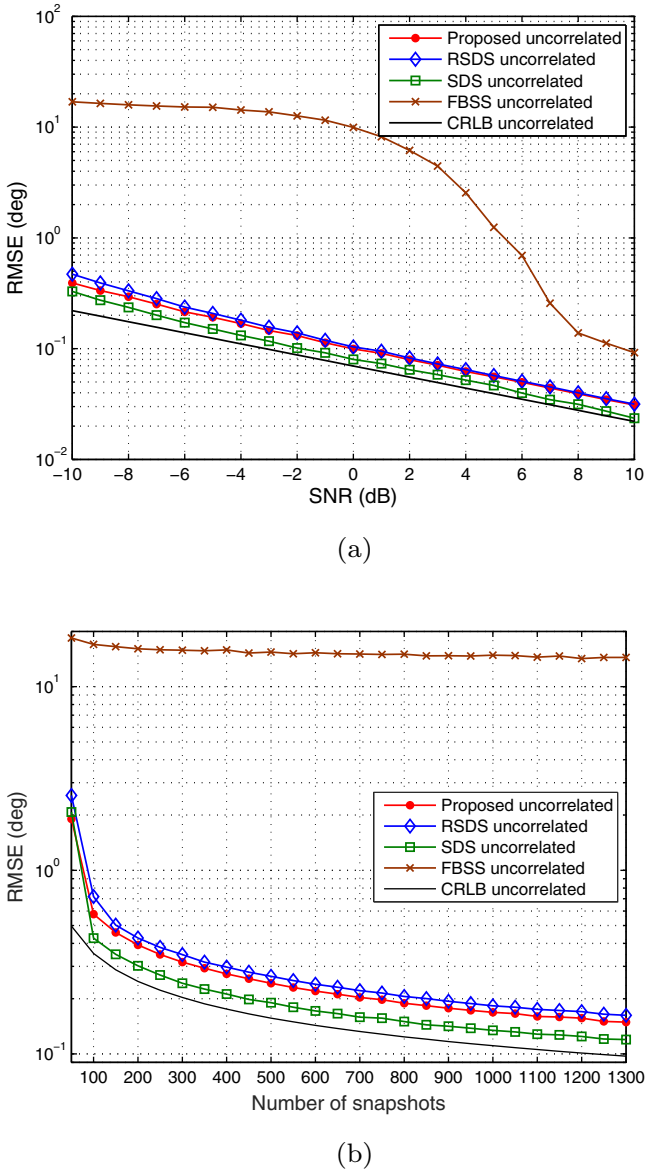

Fig. 2. RMSE of the uncorrelated signal estimates in the overdetermined case versus (a) SNR when the number of snapshots is 800; (b) the number of snapshots when SNR $= -5$ dB.

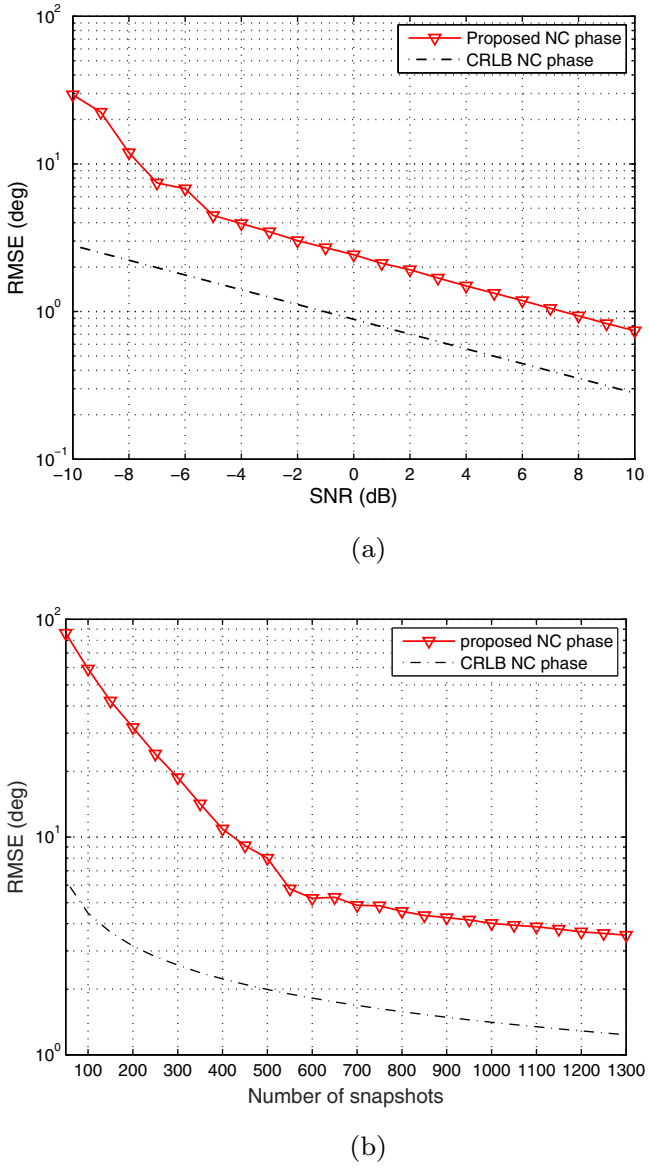

Fig. 3. RMSE of the noncircularity phase estimates for 3 uncorrelated signals. (a) The number of snapshots is 800. (b) The SNR $= -5$ dB.

4.2. Overdetermined DOA estimation and corresponding noncircularity phase estimation of uncorrelated signals

Now, the performances of the above methods are examined by a case of mixed uncorrelated and coherent signals. We consider three uncorrelated sources from $[55°,\ 16°,\ -18°]$ and a group of four coherent signals from $[-10°, -2°, 28°, 36°]$, impinging on the array. The fading coefficients of the coherent signals are $[-0.9867 - 0.1625j, -0.0438 + 0.8989j, 0.5511 + 0.4316j, -0.5914 + 0.1013j]$ where the variation of amplitudes reflect fading of different paths and the fading phases comply with the uniform distribution. The noncircularity phases are [51.55°, 259.13°, 161.93°, 164.02°] which also follow the uniform distribution. We select $m = 7$ for rank restoration of $\mathbf{R}_{xc}$. Fig. 2 depicts the RMSE of the DOA estimates of uncorrelated signals versus input SNR and the number of snapshots. Additionally, we plot the deterministic CRLB for the noncircular uncorrelated signals under multipath propagation, which is derived in Appendix E. From this figure, we can see that although the proposed method is somewhat inferior to SDS in the uncorrelated signal estimation, which is a bit surprising. The reason, we believe, is that in overdetermined case the signal (or noise) subspace obtained from eigen-decomposition is already close (or orthogonal) to the space spanned by the array manifold. As a result, the improvement made from a virtual doubling of the sensor elements cannot be very significant, whereas the margin between MUSIC- and ESPRIT-like approaches is non-negligible. With an increase in SNR, estimation accuracies of all four algorithms improve asymptotically. Although FBSS can simultaneously resolve uncorrelated and coherent signals, its performance is barely acceptable since it does not take full advantage of the array elements, compared with the two-stage-based methods. As a result, it has the worst estimation accuracy for uncorrelated signals.

The RMSE of the noncircularity phase estimates versus input SNR and number of snapshots is shown in Fig. 3. The results illustrate that the performance of noncircularity phase estimation improves with increasing SNR and number of snapshots, but there is a clear margin between the noncircularity phase estimates and the CRLB. The margin shown in Fig. 3 is mainly due to the error

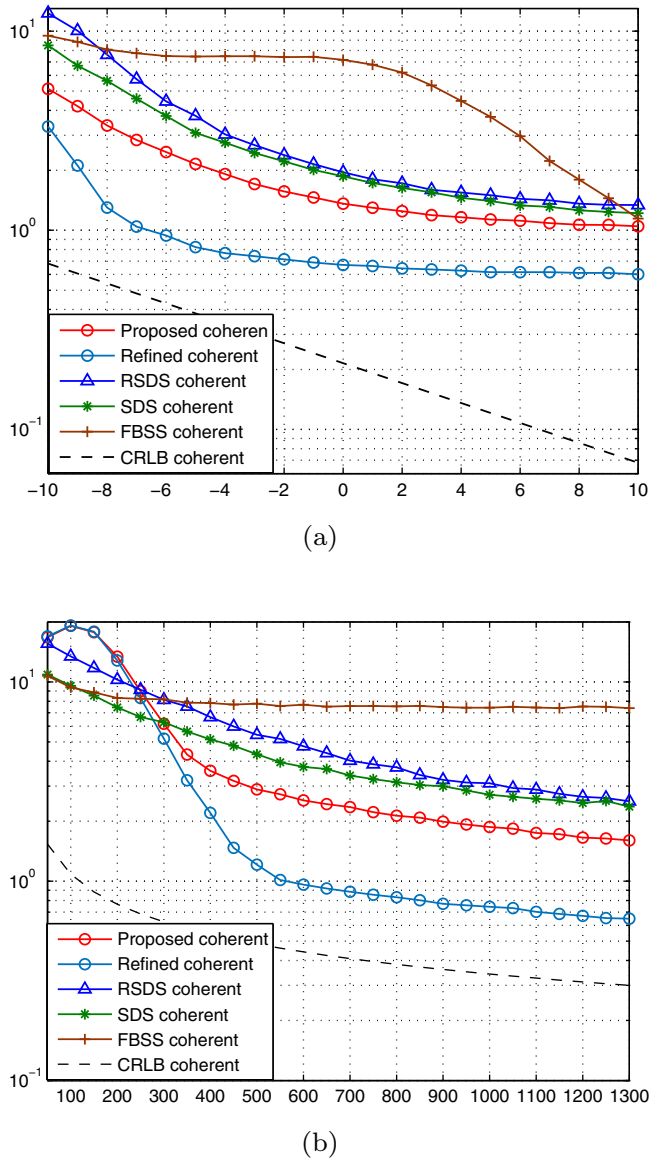

Fig. 4. RMSE of the coherent signal estimates in the overdetermined case versus (a) SNR when the number of snapshots is 800; (b) the number of snapshots when SNR = −5 dB.

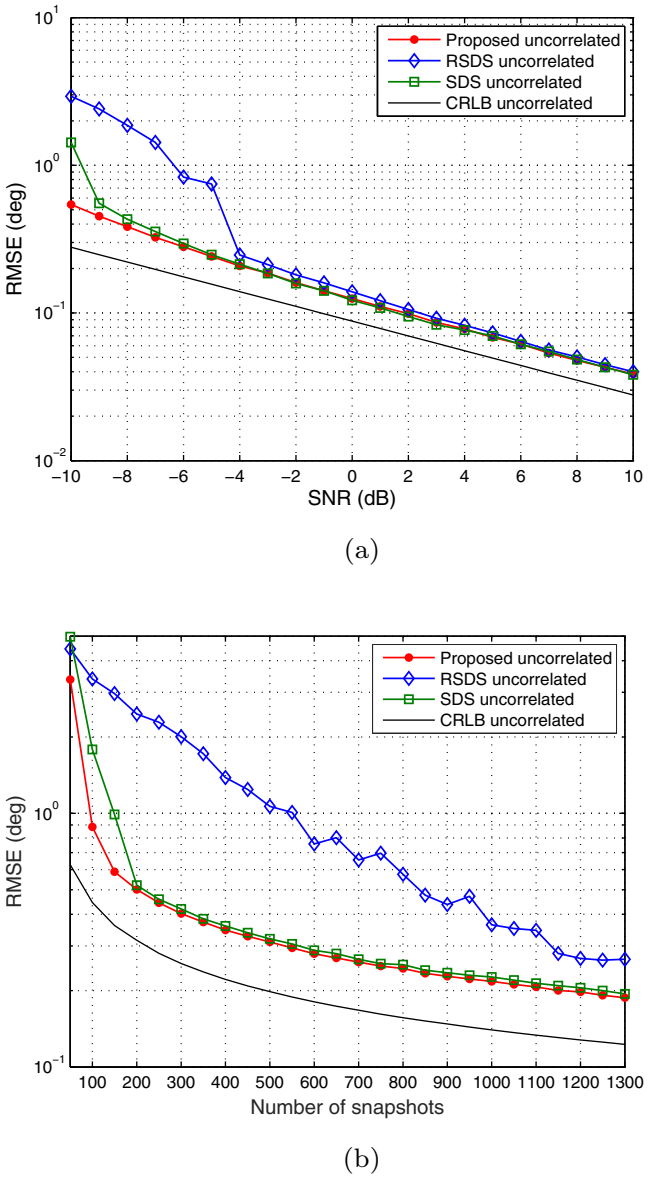

Fig. 5. RMSE of the uncorrelated signal estimates in the underdetermined case versus (a) SNR when the number of snapshots is 800; (b) the number of snapshots when SNR = −5 dB.

propagation—the estimation errors of uncorrelated signals in the first stage will be propagated to the noncircularity phase estimation.

In Fig. 4 we exhibit the RMSE performance of all four methods for the coherent signal estimation as the SNR and the number of snapshots increase. It is observed that the proposed algorithm has the lowest RMSE for coherent signals, among all the algorithms for all SNRs and snapshots larger than 300, followed by SDS, RSDS, and then FBSS. Besides, the refinement operation provides a significant performance improvement via the coarse estimates provided by the proposed method. This is mainly because, as mentioned earlier, the refinement technique exploits the full array aperture, whereas the estimation accuracy of the spatial smoothing techniques is confined to the reduced size of smoothed matrix. FBSS only ameliorates at high SNRs and has a relatively large bias for coherent signals compared with the other three algorithms even for a relatively large number of snapshots at a moderate SNR.

4.3. Underdetermined DOA estimation and corresponding noncircularity phase estimation of uncorrelated signals

We consider five uncorrelated signals from $[-41^\circ, -19^\circ, 5^\circ, 38^\circ, 50^\circ]$ and two groups of three coherent signals from $[-48^\circ, -33^\circ, -10^\circ]$ and $[14^\circ, 25^\circ, 57^\circ]$ impinging on the ULA. The fading coefficients of the coherent signals are $[0.6595 + 0.7517j, -0.4656 + 0.7702j, 0.2225 + 0.6637j]$ and $[-0.9867 - 0.1625j, 0.6500 + 0.4664j, 0.1407 - 0.5833j]$, respectively. The noncircularity phases are [51.55°, 259.13°, 161.93°, 164.02°, 40.75°, 15.19°, 263.59°]. We select $m = 7$ in this scenario.

Based on these settings, the simulation results of the RMSE of the uncorrelated signal estimates by varying SNR and the number of snapshots are illustrated in Fig. 5. The total number of signals exceeds the number of array elements, and thus FBSS fails to work. As is shown in Fig. 5, the proposed approach achieves the best performance over the range of SNR values and the number of snapshots for the uncorrelated signal estimation. Under this more challenging scenario, the proposed approach even outperforms SDS for

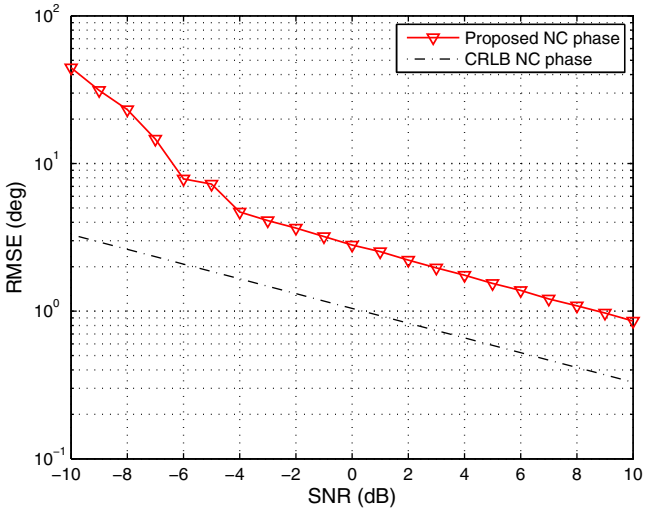

(a)

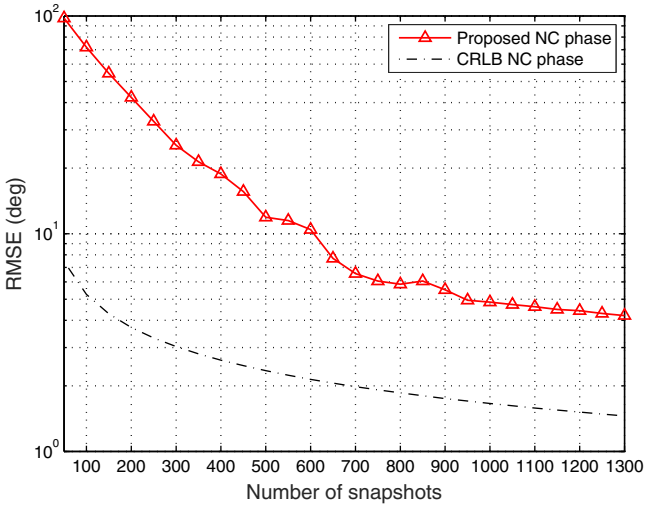

(b)

Fig. 6. RMSE of the noncircularity phase estimates for 5 uncorrelated signals. (a) The number of snapshots is 800. (b) The SNR = −5 dB.

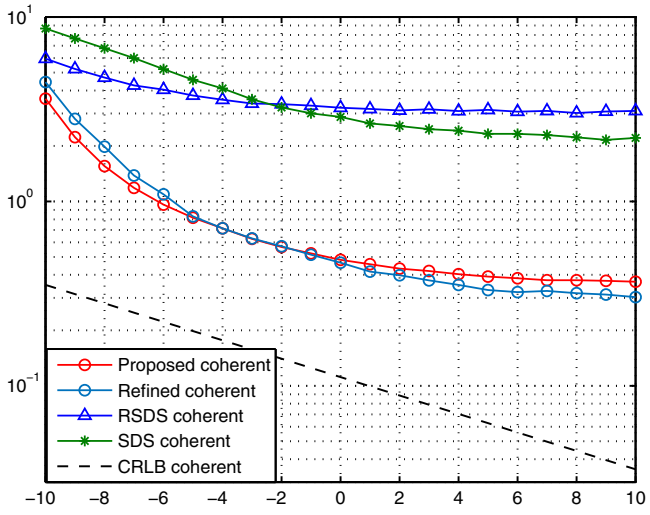

(a)

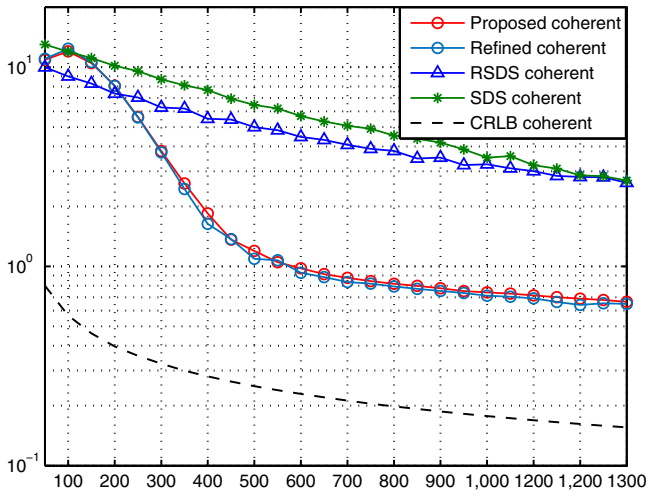

(b)

Fig. 7. RMSE of the coherent signal estimates in the underdetermined case versus (a) SNR when the number of snapshots is 800; (b) the number of snapshots when SNR = −5 dB.

the uncorrelated case, especially at low SNRs. This is because that dimension reduced noise subspace of SDS is roughly orthogonal to the array manifold, resulting in larger estimation errors, whereas the proposed method performs better because the reliable signal subspace can still be acquired from the augmented space. However, consistent with the overdetermined case, SDS is still superior to RSDS for the uncorrelated signal estimation because of its one dimensional search of the spatial spectrum. In the same scenario, the RMSE of the noncircularity phase estimates versus input SNR and number of snapshots is shown in Fig. 6. Similar to Fig. 3, the estimation errors of noncircularity phase drop with increasing SNR and number of snapshots, only with a slightly worse accuracy than that of the first scenario due to more estimations requiring to be carried out.

In Fig. 7 we plot the performance of the three methods for the coherent signal estimation as well as CRLB as a function of SNR and the total number of snapshots. It can be seen that the proposed method has a greater advantage over the other two algorithms than the first scenario shown in Fig. 4 for all SNRs and number of snapshots larger than 200, and the refinement scheme enhances the estimation accuracy slightly at high SNRs while performs a bit worse at low SNRs, which may imply that the proposed spatial smoothing method provides small DOA estimation errors that are already close to the refinement technique. Among the other approaches, the RSDS algorithm performs better than SDS for coherent signal estimation up to −2 dB, but worse above −2 dB. When fixing SNR = −5 dB, as observed in Fig. 7(b), the performance of SDS for coherent signal estimation improves faster than that of RSDS with increasing snapshots, and approaches RSDS when the number of snapshots is larger than 1100.

5. Conclusion

The DOA estimation of noncircular signals under multipath is addressed in this paper, and a two-stage DOA estimation algorithm is proposed for this case. The algorithm makes efficient use of the DOF of a ULA, and enables us to separately deal with two different types of signals, thus resolving more signals than the number of array elements. At the first stage, we construct an augmented snapshots of array outputs, then use the eigenvectors of the aug-

mented covariance matrix, corresponding to signal subspace, to resolve the uncorrelated signals with our proposed criterion. Our theoretical identifiability analysis has revealed that the proposed method can uniquely make a reasonable classification of the source types. After the first stage, the uncorrelated components are removed from the covariance matrix of the augmented data based on the DOA and noncircularity phase estimates of the uncorrelated sources. Then, a spatial smoothing on the denoised covariance matrix is performed to restore the rank deficiency in the covariance matrix of the coherent signals, and finally their DOAs are resolved using a similar procedure as for uncorrelated sources. Compared with previous two-stage-based methods, the proposed solution is efficient in the sense that by exploitation of the noncircularity of the incident signals it achieves a more reasonable classification of the signal types, alleviates the array DOF and aperture loss, as well as improving the estimation accuracy of both uncorrelated and coherent signals. And more robust under adverse noise conditions (SNR) and data availability (i.e., snapshots).

Appendix A. Proof of (6)

Proof. If defining $\tilde{\mathbf{\Gamma}}_u = \begin{bmatrix} \mathbf{\Phi}_u^{1-M}\mathbf{\Psi}_u^* \\ \mathbf{\Psi}_u \end{bmatrix}$, to relate $\mathbf{U}_{s2}$ to $\mathbf{A}_{c1}$ and $\tilde{\mathbf{A}}_{u1}$, we start with the transformation of $\mathbf{U}_{s2}$ as

$$\begin{aligned}
\mathbf{U}_{s2} &= (\mathbf{I}_2 \otimes \mathbf{J}_2)\mathbf{U}_s = \begin{bmatrix} (\mathbf{I}_2 \otimes \mathbf{J}_2)\tilde{\mathbf{A}}_c, (\mathbf{I}_2 \otimes \mathbf{J}_2)\tilde{\mathbf{A}}_u \end{bmatrix}\mathbf{T} \\
&= \begin{bmatrix} (\mathbf{I}_2 \otimes \mathbf{J}_2)(\mathbf{I}_2 \otimes \mathbf{A}_c)\tilde{\mathbf{\Gamma}}_c, (\mathbf{I}_2 \otimes \mathbf{J}_2)(\mathbf{I}_2 \otimes \mathbf{A}_u)\tilde{\mathbf{\Gamma}}_u \end{bmatrix}\mathbf{T} \\
&= \begin{bmatrix} (\mathbf{I}_2 \otimes \mathbf{J}_2\mathbf{A}_c)\tilde{\mathbf{\Gamma}}_c, (\mathbf{I}_2 \otimes \mathbf{J}_2\mathbf{A}_u)\tilde{\mathbf{\Gamma}}_u \end{bmatrix}\mathbf{T} \\
&= \begin{bmatrix} (\mathbf{I}_2 \otimes \mathbf{J}_1\mathbf{A}_c\mathbf{\Phi}_c)\tilde{\mathbf{\Gamma}}_c, (\mathbf{I}_2 \otimes \mathbf{J}_1\mathbf{A}_u\mathbf{\Phi}_u)\tilde{\mathbf{\Gamma}}_u \end{bmatrix}\mathbf{T} \\
&= \begin{bmatrix} (\mathbf{I}_2 \otimes \mathbf{J}_1\mathbf{A}_c)(\mathbf{I}_2 \otimes \mathbf{\Phi}_c)\tilde{\mathbf{\Gamma}}_c, (\mathbf{I}_2 \otimes \mathbf{J}_1\mathbf{A}_u)(\mathbf{I}_2 \otimes \mathbf{\Phi}_u)\tilde{\mathbf{\Gamma}}_u \end{bmatrix}\mathbf{T} \\
&= \begin{bmatrix} (\mathbf{I}_2 \otimes \mathbf{A}_{c1})\tilde{\mathbf{\Phi}}_c\tilde{\mathbf{\Gamma}}_c, (\mathbf{I}_2 \otimes \mathbf{A}_{u1})\tilde{\mathbf{\Gamma}}_u\mathbf{\Phi}_u \end{bmatrix}\mathbf{T} \\
&= \begin{bmatrix} (\mathbf{I}_2 \otimes \mathbf{A}_{c1})\tilde{\mathbf{\Phi}}_c\tilde{\mathbf{\Gamma}}_c, \tilde{\mathbf{A}}_{u1}\mathbf{\Phi}_u \end{bmatrix}\mathbf{T}
\end{aligned} \tag{A.1}$$

where in the third equality we have used $\tilde{\mathbf{A}}_c = (\mathbf{I}_2 \otimes \mathbf{A}_c)\tilde{\mathbf{\Gamma}}_c$, in the fifth equality we have used the shift invariance equations $\mathbf{J}_1\mathbf{A}_c\mathbf{\Phi}_c = \mathbf{J}_2\mathbf{A}_c$ and $\mathbf{J}_1\mathbf{A}_u\mathbf{\Phi}_u = \mathbf{J}_2\mathbf{A}_u$, respectively, in the seventh equality we have used $(\mathbf{I}_2 \otimes \mathbf{\Phi}_u)\tilde{\mathbf{\Gamma}}_u = \tilde{\mathbf{\Gamma}}_u\mathbf{\Phi}_u$ which is only due to the fact that $\tilde{\mathbf{\Gamma}}_u$ consists of diagonal matrices which permute, namely,

$$\begin{aligned}
(\mathbf{I}_2 \otimes \mathbf{\Phi}_u)\tilde{\mathbf{\Gamma}}_u &= (\mathbf{I}_2 \otimes \mathbf{\Phi}_u)\begin{bmatrix} \mathbf{\Phi}_u^{1-M}\mathbf{\Psi}_u^* \\ \mathbf{\Psi}_u \end{bmatrix} \\
&= \begin{bmatrix} \mathbf{\Phi}_u\mathbf{\Phi}_u^{1-M}\mathbf{\Psi}_u^* \\ \mathbf{\Phi}_u\mathbf{\Psi}_u \end{bmatrix} = \begin{bmatrix} \mathbf{\Phi}_u^{1-M}\mathbf{\Psi}_u^*\mathbf{\Phi}_u \\ \mathbf{\Psi}_u\mathbf{\Phi}_u \end{bmatrix} = \tilde{\mathbf{\Gamma}}_u\mathbf{\Phi}_u.
\end{aligned} \tag{A.2}$$

As a result, one has

$$\begin{aligned}
\mathbf{U}_{s1}^{+}\mathbf{U}_{s2} &= \mathbf{T}^{-1}\begin{bmatrix} \tilde{\mathbf{A}}_{c1}, \tilde{\mathbf{A}}_{u1} \end{bmatrix}^{+}\begin{bmatrix} \tilde{\mathbf{A}}_{c2}, \tilde{\mathbf{A}}_{u1}\mathbf{\Phi}_u \end{bmatrix}\mathbf{T} \\
&= \mathbf{T}^{-1}\left(\begin{bmatrix} (\mathbf{I}_2 \otimes \mathbf{A}_{c1})\tilde{\mathbf{\Gamma}}_c, \tilde{\mathbf{A}}_{u1} \end{bmatrix}^H\begin{bmatrix} (\mathbf{I}_2 \otimes \mathbf{A}_{c1})\tilde{\mathbf{\Gamma}}_c, \tilde{\mathbf{A}}_{u1} \end{bmatrix}\right)^{-1} \\
&\quad \times \begin{bmatrix} (\mathbf{I}_2 \otimes \mathbf{A}_{c1})\tilde{\mathbf{\Gamma}}_c, \tilde{\mathbf{A}}_{u1} \end{bmatrix}^H\begin{bmatrix} (\mathbf{I}_2 \otimes \mathbf{A}_{c1})\tilde{\mathbf{\Phi}}_c\tilde{\mathbf{\Gamma}}_c, \tilde{\mathbf{A}}_{u1}\mathbf{\Phi}_u \end{bmatrix}\mathbf{T} \\
&= \mathbf{T}^{-1}\begin{bmatrix} \tilde{\mathbf{\Gamma}}_c^H\left(\mathbf{I}_2 \otimes \left(\mathbf{A}_{c1}^H\mathbf{A}_{c1}\right)\right)\tilde{\mathbf{\Gamma}}_c & \tilde{\mathbf{\Gamma}}_c^H\left(\mathbf{I}_2 \otimes \mathbf{A}_{c1}^H\right)\tilde{\mathbf{A}}_{u1} \\ \tilde{\mathbf{A}}_{u1}^H(\mathbf{I}_2 \otimes \mathbf{A}_{c1})\tilde{\mathbf{\Gamma}}_c & \tilde{\mathbf{A}}_{u1}^H\tilde{\mathbf{A}}_{u1} \end{bmatrix}^{-1} \\
&\quad \times \begin{bmatrix} \tilde{\mathbf{\Gamma}}_c^H\left(\mathbf{I}_2 \otimes \left(\mathbf{A}_{c1}^H\mathbf{A}_{c1}\right)\right)\tilde{\mathbf{\Phi}}_c\tilde{\mathbf{\Gamma}}_c & \tilde{\mathbf{\Gamma}}_c^H\left(\mathbf{I}_2 \otimes \mathbf{A}_{c1}^H\right)\tilde{\mathbf{A}}_{u1}\mathbf{\Phi}_u \\ \tilde{\mathbf{A}}_{u1}^H(\mathbf{I}_2 \otimes \mathbf{A}_{c1})\tilde{\mathbf{\Phi}}_c\tilde{\mathbf{\Gamma}}_c & \tilde{\mathbf{A}}_{u1}^H\tilde{\mathbf{A}}_{u1}\mathbf{\Phi}_u \end{bmatrix}\mathbf{T} \\
&= \mathbf{T}^{-1}\begin{bmatrix} \tilde{\mathbf{\Gamma}}_c^H\left(\mathbf{I}_2 \otimes \left(\mathbf{A}_{c1}^H\mathbf{A}_{c1}\right)\right)\tilde{\mathbf{\Gamma}}_c & \tilde{\mathbf{\Gamma}}_c^H\left(\mathbf{I}_2 \otimes \mathbf{A}_{c1}^H\right)\tilde{\mathbf{A}}_{u1} \\ \tilde{\mathbf{A}}_{u1}^H(\mathbf{I}_2 \otimes \mathbf{A}_{c1})\tilde{\mathbf{\Gamma}}_c & \tilde{\mathbf{A}}_{u1}^H\tilde{\mathbf{A}}_{u1} \end{bmatrix}^{-1} \\
&\quad \times \begin{bmatrix} \tilde{\mathbf{\Gamma}}_c^H\left(\mathbf{I}_2 \otimes \left(\mathbf{A}_{c1}^H\mathbf{A}_{c1}\right)\right)\tilde{\mathbf{\Gamma}}_c & \tilde{\mathbf{\Gamma}}_c^H\left(\mathbf{I}_2 \otimes \mathbf{A}_{c1}^H\right)\tilde{\mathbf{A}}_{u1} \\ \tilde{\mathbf{A}}_{u1}^H(\mathbf{I}_2 \otimes \mathbf{A}_{c1})\tilde{\mathbf{\Gamma}}_c & \tilde{\mathbf{A}}_{u1}^H\tilde{\mathbf{A}}_{u1} \end{bmatrix} \\
&\quad \times \begin{bmatrix} \mathbf{F}_1 & \mathbf{0}_{K\times N_u} \\ \mathbf{F}_2 & \mathbf{\Phi}_u \end{bmatrix}\mathbf{T} \\
&= \mathbf{T}^{-1}\begin{bmatrix} \mathbf{F}_1 & \mathbf{0}_{K\times N_u} \\ \mathbf{F}_2 & \mathbf{\Phi}_u \end{bmatrix}\mathbf{T}
\end{aligned} \tag{A.3}$$

and this proves (6). □

Appendix B. Analysis of eigenvalues of block lower triangular matrix

By definition, an eigenvalue η of the block matrix $\begin{bmatrix} \mathbf{F}_1 & \mathbf{0}_{K\times N_u} \\ \mathbf{F}_2 & \mathbf{\Phi}_u \end{bmatrix}$ satisfies $\det\left\{\begin{bmatrix} \mathbf{F}_1 & \mathbf{0}_{K\times N_u} \\ \mathbf{F}_2 & \mathbf{\Phi}_u \end{bmatrix} - \eta\mathbf{I}_{K+N_u}\right\} = \det\left\{\begin{bmatrix} \mathbf{F}_1 - \eta\mathbf{I}_K & \mathbf{0}_{K\times N_u} \\ \mathbf{F}_2 & \mathbf{\Phi}_u - \eta\mathbf{I}_{N_u} \end{bmatrix}\right\} = 0$. Using the identity $\det\left\{\begin{bmatrix} \mathbf{B}_{1,1} & \mathbf{0}_{m\times n} \\ \mathbf{B}_{2,1} & \mathbf{B}_{2,2} \end{bmatrix}\right\} = \det\{\mathbf{B}_{1,1}\}\det\{\mathbf{B}_{2,2}\}$ where $\mathbf{B}_{1,1} \in \mathbb{C}^{m\times m}$, $\mathbf{B}_{2,1} \in \mathbb{C}^{n\times m}$, and $\mathbf{B}_{2,2} \in \mathbb{C}^{n\times n}$, one has $\det\left\{\begin{bmatrix} \mathbf{F}_1 & \mathbf{0}_{K\times N_u} \\ \mathbf{F}_2 & \mathbf{\Phi}_u \end{bmatrix} - \eta\mathbf{I}_{K+N_u}\right\} = \det\{\mathbf{F}_1 - \eta\mathbf{I}_K\}\det\left\{\mathbf{\Phi}_u - \eta\mathbf{I}_{N_u}\right\} = 0$. Thus we say that if η is an eigenvalue of $\begin{bmatrix} \mathbf{F}_1 & \mathbf{0}_{K\times N_u} \\ \mathbf{F}_2 & \mathbf{\Phi}_u \end{bmatrix}$, then either $\det\{\mathbf{F}_1 - \eta\mathbf{I}_K\} = 0$ or $\det\left\{\mathbf{\Phi}_u - \eta\mathbf{I}_{N_u}\right\} = 0$ and, hence η is also an eigenvalue of $\mathbf{F}_1$ or $\mathbf{\Phi}_u$.

Appendix C. Proof of (16)

Proof. Performing the compact singular value decomposition (SVD) of $\bar{\mathbf{A}} \triangleq \begin{bmatrix} \tilde{\mathbf{A}}_c, \tilde{\mathbf{A}}_u \end{bmatrix} = \begin{bmatrix} \mathbf{E}_1, \tilde{\mathbf{a}}(\theta_i, \phi_i), \mathbf{E}_2 \end{bmatrix}, i = K+1, \ldots, K+N_u$, where $\mathbf{E}_1$ and $\mathbf{E}_2$ are the remaining parts of $\bar{\mathbf{A}}$ except $\tilde{\mathbf{a}}(\theta_i, \phi_i)$, we have

$$\bar{\mathbf{A}} = \sum_{k=1}^{K+N_u} \eta_k\mathbf{u}_k\mathbf{v}_k^H \tag{C.1}$$

where $\{\eta_k\}_{k=1}^{K+N_u}, \{\mathbf{u}_k\}_{k=1}^{K+N_u}, \{\mathbf{v}_k\}_{k=1}^{K+N_u}$ are the non-zero singular values, left singular vectors, and right singular vectors, respectively. Accordingly, the pseudo-inverse of $\bar{\mathbf{A}}$ is

$$\bar{\mathbf{A}}^{+} = \sum_{k=1}^{K+N_u} \eta_k^{-1}\mathbf{v}_k\mathbf{u}_k^H. \tag{C.2}$$

Since $\tilde{\mathbf{R}} - \sigma_n^2\mathbf{I} = \bar{\mathbf{A}}\mathbf{R}_0\bar{\mathbf{A}}^H$ where $\mathbf{R}_0 = \mathrm{diag}\left\{\sigma_1^2, \sigma_2^2, \ldots, \sigma_{K+N_u}^2\right\}$, and $\mathbf{b}(\theta, \phi) = e^{j\frac{\phi}{2}}\tilde{\mathbf{a}}(\theta, \phi)$, this allows us to expand the term

$$\begin{aligned}
&\mathbf{b}^H(\theta_i, \phi_i)\left(\tilde{\mathbf{R}} - \sigma_n^2\mathbf{I}\right)^{+}\mathbf{b}(\theta_i, \phi_i) \\
&\quad = \tilde{\mathbf{a}}^H(\theta_i, \phi_i)\left(\bar{\mathbf{A}}^H\right)^{+}\mathbf{R}_0^{-1}\bar{\mathbf{A}}^{+}\tilde{\mathbf{a}}(\theta_i, \phi_i) \\
&\quad = \left(\bar{\mathbf{A}}^{+}\tilde{\mathbf{a}}(\theta_i, \phi_i)\right)^H\mathbf{R}_0^{-1}\bar{\mathbf{A}}^{+}\tilde{\mathbf{a}}(\theta_i, \phi_i).
\end{aligned} \tag{C.3}$$

Note that $\tilde{\mathbf{a}}(\theta_i, \phi_i) = \bar{\mathbf{A}}\mathbf{e}_i$ where $\mathbf{e}_i \in \mathbb{R}^{K+N_u}$ is a column vector with 1 at the ith entry and 0 elsewhere, then substitute it back to (C.3),

$$\begin{aligned}
&\mathbf{b}^H(\theta_i, \phi_i)\left(\tilde{\mathbf{R}} - \sigma_n^2\mathbf{I}\right)^{+}\mathbf{b}(\theta_i, \phi_i) \\
&\quad = \left(\sum_{k=1}^{K+N_u} \eta_k^{-1}\mathbf{v}_k\mathbf{u}_k^H\sum_{k=1}^{K+N_u} \eta_k\mathbf{u}_k\mathbf{v}_k^H\mathbf{e}_i\right)^H\mathbf{R}_0^{-1} \\
&\qquad \times \sum_{k=1}^{K+N_u} \eta_k^{-1}\mathbf{v}_k\mathbf{u}_k^H\sum_{k=1}^{K+N_u} \eta_k\mathbf{u}_k\mathbf{v}_k^H\mathbf{e}_i
\end{aligned}$$

$$= \mathbf{e}_i^H \mathbf{R}_0^{-1} \mathbf{e}_i$$
$$= \mathbf{e}_i^H \mathrm{diag}\{\sigma_1^{-2}, \sigma_2^{-2}, \ldots, \sigma_{K+N_u}^{-2}\}\mathbf{e}_i$$
$$= \sigma_i^{-2}. \tag{C.4}$$

Therefore,

$$\sigma_i^2 = \frac{1}{\mathbf{b}^H(\theta_i, \phi_i)\left(\tilde{\mathbf{R}} - \sigma_n^2 \mathbf{I}\right)^+ \mathbf{b}(\theta_i, \phi_i)}, \quad i = K+1, \ldots, K+N_u \tag{C.5}$$

and this proves (16). □

Appendix D. Proof of Proposition 1

Proof. Under the assumptions that $\mathbf{A}_c$ is unambiguous and $m \geq N_c + 1$, the rank of the Vandermonde matrix $\mathbf{B}_c$ is given by $\mathrm{rank}(\mathbf{B}_c) = N_c$. If we define

$$\mathbf{G}_i = \frac{1}{q}\sum_{r=1}^{q}\left(\mathbf{I}_2 \otimes \bar{\mathbf{J}}_r\right)\tilde{\mathbf{A}}_c \boldsymbol{\beta}_i \boldsymbol{\beta}_i^H \tilde{\mathbf{A}}_c^H \left(\mathbf{I}_2 \otimes \bar{\mathbf{J}}_r^T\right) \tag{D.1}$$

where $\boldsymbol{\beta}_i = [\beta_{i1}, \beta_{i2}, \ldots, \beta_{iK}]^T \in \mathbb{C}^K$ is the ith column vector of $\tilde{\mathbf{T}}$, since $\left(\mathbf{I}_2 \otimes \bar{\mathbf{J}}_r\right)\tilde{\mathbf{A}}_c = \begin{bmatrix} \mathbf{B}_c \boldsymbol{\Phi}_c^{r-M} \boldsymbol{\Gamma}^* \boldsymbol{\Psi}_c^* \\ \mathbf{B}_c \boldsymbol{\Phi}_c^{r-1} \boldsymbol{\Gamma} \boldsymbol{\Psi}_c \end{bmatrix}$ where $\mathbf{B}_c = \mathbf{F}\left[\mathbf{A}_{c,1}, \mathbf{A}_{c,2}, \ldots, \mathbf{A}_{c,K}\right]$ with $\mathbf{F} = \begin{bmatrix} \mathbf{I}_{(M-p+1)}, \mathbf{0}_{(M-p+1)\times(p-1)} \end{bmatrix}$, $\mathbf{G}_i$ can be rewritten as

$$\begin{aligned}
\mathbf{G}_i &= \frac{1}{q}\sum_{r=1}^{q}\begin{bmatrix} \mathbf{B}_c \boldsymbol{\Phi}_c^{r-M} \boldsymbol{\Gamma}^* \boldsymbol{\Psi}_c^* \\ \mathbf{B}_c \boldsymbol{\Phi}_c^{r-1} \boldsymbol{\Gamma} \boldsymbol{\Psi}_c \end{bmatrix} \boldsymbol{\beta}_i \boldsymbol{\beta}_i^H \begin{bmatrix} \mathbf{B}_c \boldsymbol{\Phi}_c^{r-M} \boldsymbol{\Gamma}^* \boldsymbol{\Psi}_c^* \\ \mathbf{B}_c \boldsymbol{\Phi}_c^{r-1} \boldsymbol{\Gamma} \boldsymbol{\Psi}_c \end{bmatrix}^H \\
&= \begin{bmatrix} \mathbf{B}_c \boldsymbol{\Phi}_c^{1-M} \boldsymbol{\Gamma}^* \boldsymbol{\Psi}_c^* \boldsymbol{\beta}_i, \mathbf{B}_c \boldsymbol{\Phi}_c^{2-M} \boldsymbol{\Gamma}^* \boldsymbol{\Psi}_c^* \boldsymbol{\beta}_i, \ldots, \mathbf{B}_c \boldsymbol{\Phi}_c^{p-M} \boldsymbol{\Gamma}^* \boldsymbol{\Psi}_c^* \boldsymbol{\beta}_i \\ \mathbf{B}_c \boldsymbol{\Gamma} \boldsymbol{\Psi}_c \boldsymbol{\beta}_i, \mathbf{B}_c \boldsymbol{\Phi}_c \boldsymbol{\Gamma} \boldsymbol{\Psi}_c \boldsymbol{\beta}_i, \ldots, \mathbf{B}_c \boldsymbol{\Phi}_c^{p-1} \boldsymbol{\Gamma} \boldsymbol{\Psi}_c \boldsymbol{\beta}_i \end{bmatrix} \\
&\quad \times \begin{bmatrix} \mathbf{B}_c \boldsymbol{\Phi}_c^{1-M} \boldsymbol{\Gamma}^* \boldsymbol{\Psi}_c^* \boldsymbol{\beta}_i, \mathbf{B}_c \boldsymbol{\Phi}_c^{2-M} \boldsymbol{\Gamma}^* \boldsymbol{\Psi}_c^* \boldsymbol{\beta}_i, \ldots, \mathbf{B}_c \boldsymbol{\Phi}_c^{p-M} \boldsymbol{\Gamma}^* \boldsymbol{\Psi}_c^* \boldsymbol{\beta}_i \\ \mathbf{B}_c \boldsymbol{\Gamma} \boldsymbol{\Psi}_c \boldsymbol{\beta}_i, \mathbf{B}_c \boldsymbol{\Phi}_c \boldsymbol{\Gamma} \boldsymbol{\Psi}_c \boldsymbol{\beta}_i, \ldots, \mathbf{B}_c \boldsymbol{\Phi}_c^{p-1} \boldsymbol{\Gamma} \boldsymbol{\Psi}_c \boldsymbol{\beta}_i \end{bmatrix}^H \\
&= \begin{bmatrix} \mathbf{B}_c \boldsymbol{\Phi}_c^{1-M} \mathbf{D}^* \mathbf{H}_i \\ \mathbf{B}_c \mathbf{D} \mathbf{H}_i \end{bmatrix} \mathbf{V}\mathbf{V}^H \begin{bmatrix} \mathbf{B}_c \boldsymbol{\Phi}_c^{1-M} \mathbf{D}^* \mathbf{H}_i \\ \mathbf{B}_c \mathbf{D} \mathbf{H}_i \end{bmatrix}^H \\
&\triangleq \tilde{\mathbf{B}}_{ci} \mathbf{V}\mathbf{V}^H \tilde{\mathbf{B}}_{ci}^H
\end{aligned} \tag{D.2}$$

where $\mathbf{D} = \mathrm{diag}\{d_{11}, \ldots, d_{1P_1}, \ldots, d_{K1}, \ldots, d_{KP_K}\}$ with $d_{kp_k} = \alpha_{kp_k} e^{j\frac{\phi_k}{2}}$, $\mathbf{H}_i = \mathrm{blkdiag}\{\mathbf{h}_{i1}, \mathbf{h}_{i2}, \ldots, \mathbf{h}_{iK}\}$ with $\mathbf{h}_{ik} = \mathrm{diag}\{\beta_{ik}, \beta_{ik}, \ldots, \beta_{ik}\} \in \mathbb{C}^{P_k \times P_k}$, and $\mathbf{V} = \mathbf{A}_c^T(1:p, 1:N_c)$. It is easy to identify that $\mathrm{rank}(\boldsymbol{\Phi}_c) = \mathrm{rank}(\mathbf{D}) = \mathrm{rank}(\mathbf{H}_i) = N_c$, $\mathrm{rank}(\mathbf{V}) = \min(N_c, p)$. Since the row vectors of $\mathbf{B}_c \boldsymbol{\Phi}_c^{1-M}$ and $\mathbf{B}_c$ are linearly independent to each other, one has $\mathrm{rank}\left(\tilde{\mathbf{B}}_{ci}\right) = \min\{2m, N_c\} = N_c$ and $\mathrm{rank}(\mathbf{G}_i) = \min\{N_c, p\} \geq P_{\max}$. Further, we know that $\tilde{\mathbf{T}}$ is of full column rank, which implies that $\{\boldsymbol{\beta}_i\}_{i=1}^K$ are linearly independent to each other, and $\mathbf{R}_{ss} = \sum_{i=1}^K \mathbf{G}_i$, so $\mathrm{rank}(\mathbf{R}_{ss}) = \min\{N_c, Kp\} = N_c$, which means that the rank deficiency in $\mathbf{R}_{xc}$ has been completely restored. This completes the proof of Proposition 1. □

Appendix E. Derivation of deterministic CRLB for the noncircular signals in the presence of multipath

In the problem of direction finding of noncircular signals under multipath propagation, the vector including all unknown parameters is

$$\boldsymbol{\eta} = \left[\boldsymbol{\theta}^T, \boldsymbol{\alpha}^T, \boldsymbol{\phi}^T, \mathbf{s}_0^T(1), \ldots, \mathbf{s}_0^T(L), \sigma_n^2\right]^T \tag{E.1}$$

where $\boldsymbol{\theta}, \boldsymbol{\alpha}, \boldsymbol{\phi}, \mathbf{s}_0(1), \ldots, \mathbf{s}_0(L)$ are the vectors of unknown DOAs, fading coefficients, noncircularity phases, signal snapshots, respectively, and σ_n^2 is the unknown noise power.

In the deterministic case, the (m, n)th entry of the Fisher information matrix (FIM) is given by Stoica and Nehorai [24]

$$\mathbf{F}_{mn} = \sum_{i=1}^{L} \mathrm{tr}\left\{\mathbf{R}_n^{-1}\frac{\partial \mathbf{R}_n}{\partial \boldsymbol{\eta}_m}\mathbf{R}_n^{-1}\frac{\partial \mathbf{R}_n}{\partial \boldsymbol{\eta}_n}\right\} + 2\sum_{i=1}^{L}\mathrm{Re}\left\{\frac{\partial \mathbf{y}^H}{\partial \boldsymbol{\eta}_m}\mathbf{R}_n^{-1}\frac{\partial \mathbf{y}}{\partial \boldsymbol{\eta}_n}\right\} \tag{E.2}$$

where $\mathbf{R}_n = \sigma_n^2 \mathbf{I}$ and the $M \times 1$ vector

$$\begin{aligned}
\mathbf{y} &= \mathbf{A}\boldsymbol{\Upsilon}\boldsymbol{\Psi}\mathbf{s}_0(i) \\
&= \mathbf{A}_c \boldsymbol{\Gamma} \boldsymbol{\Psi}_c \mathbf{s}_{c,0}(i) + \mathbf{A}_u \boldsymbol{\Psi}_u \mathbf{s}_{u,0}(i).
\end{aligned} \tag{E.3}$$

For convenience of formulation, we define the following notations:

$$\dot{\mathbf{A}} = \left[\left.\frac{d\mathbf{a}(\theta)}{d\theta}\right|_{\theta=\theta_1}, \left.\frac{d\mathbf{a}(\theta)}{d\theta}\right|_{\theta=\theta_2}, \ldots, \left.\frac{d\mathbf{a}(\theta)}{d\theta}\right|_{\theta=\theta_N}\right] \tag{E.4}$$

$$\boldsymbol{\Pi} = \mathrm{blkdiag}\{\mathbf{1}_{P_1}, \mathbf{1}_{P_2}, \ldots, \mathbf{1}_{P_k}\} \tag{E.5}$$

$$\dot{\boldsymbol{\Psi}} = \mathrm{diag}\left\{\left.\frac{de^{j\frac{\phi}{2}}}{d\phi}\right|_{\phi=\phi_1}, \left.\frac{de^{j\frac{\phi}{2}}}{d\phi}\right|_{\phi=\phi_2}, \ldots, \left.\frac{de^{j\frac{\phi}{2}}}{d\phi}\right|_{\phi=\phi_{K+N_u}}\right\} \tag{E.6}$$

$$\hat{\mathbf{P}} = \frac{1}{L}\sum_{t=1}^{L}\mathbf{s}_0(i)\mathbf{s}_0^H(i) \tag{E.7}$$

$$\hat{\mathbf{P}}_c = \frac{1}{L}\sum_{i=1}^{L}\mathbf{s}_{c,0}(i)\mathbf{s}_{c,0}^H(i) \tag{E.8}$$

$$\hat{\mathbf{P}}_d = \frac{1}{L}\sum_{i=1}^{L}\mathbf{s}_{c,0}(i)\mathbf{s}_0^H(i) \tag{E.9}$$

$$\begin{aligned}
\mathbf{Q}(i) = \mathrm{diag}\Big\{&\alpha_{11}e^{j\frac{\phi_1}{2}}s_{1,0}(i), \ldots, \alpha_{1P_1}e^{j\frac{\phi_1}{2}}s_{1,0}(i), \ldots, \\
&\alpha_{K1}e^{j\frac{\phi_K}{2}}s_{K,0}(i), \ldots, \alpha_{KP_K}e^{j\frac{\phi_K}{2}}s_{K,0}(i), \\
&e^{j\frac{\phi_{K+1}}{2}}s_{K+1,0}(i), \ldots, e^{j\frac{\phi_{K+N_u}}{2}}s_{K+N_u,0}(i)\Big\}
\end{aligned} \tag{E.10}$$

$$\begin{aligned}
\mathbf{Q}_c(i) = \mathrm{diag}\Big\{&\alpha_{11}e^{j\frac{\phi_1}{2}}s_{1,0}(i), \ldots, \alpha_{1P_1}e^{j\frac{\phi_1}{2}}s_{1,0}(i), \ldots, \\
&\alpha_{K1}e^{j\frac{\phi_K}{2}}s_{K,0}(i), \ldots, \alpha_{KP_K}e^{j\frac{\phi_K}{2}}s_{K,0}(i)\Big\}
\end{aligned} \tag{E.11}$$

$$\mathbf{W}(i) = \mathrm{diag}\{s_{1,0}(i), s_{2,0}(i), \ldots, s_{K+N_u,0}(i)\} \tag{E.12}$$

where $\mathbf{1}_l$ is a $l \times 1$ vector with all the entries being 1. Additionally, define $\boldsymbol{\mu} = \mathrm{Re}\{\boldsymbol{\alpha}\}$ and $\boldsymbol{\nu} = \mathrm{Im}\{\boldsymbol{\alpha}\}$.

In this appendix, all blocks of the FIM corresponding to the unknown parameters required to calculate the CRLB are derived. The idea behind the derivation can be found in [24,25], and hence the detailed derivations are omitted here for simplicity.

$$\mathbf{F}_{\boldsymbol{\theta}\boldsymbol{\theta}} = \frac{2L}{\sigma_n^2}\mathrm{Re}\left\{\left(\dot{\mathbf{A}}^H\dot{\mathbf{A}}\right) \odot \left(\boldsymbol{\Upsilon}\boldsymbol{\Psi}\hat{\mathbf{P}}\boldsymbol{\Psi}^H\boldsymbol{\Upsilon}^H\right)^T\right\} \tag{E.13}$$

$$\mathbf{F}_{\boldsymbol{\mu}\boldsymbol{\mu}} = \frac{2L}{\sigma_n^2}\mathrm{Re}\left\{\left(\mathbf{A}_c^H\mathbf{A}_c\right) \odot \left(\boldsymbol{\Pi}\boldsymbol{\Psi}_c\hat{\mathbf{P}}_c\boldsymbol{\Psi}_c^H\boldsymbol{\Pi}^H\right)^T\right\} \tag{E.14}$$

$$\mathbf{F}_{\boldsymbol{\nu}\boldsymbol{\nu}} = \frac{2L}{\sigma_n^2}\mathrm{Re}\left\{\left(\mathbf{A}_c^H\mathbf{A}_c\right) \odot \left(\boldsymbol{\Pi}\boldsymbol{\Psi}_c\hat{\mathbf{P}}_c\boldsymbol{\Psi}_c^H\boldsymbol{\Pi}^H\right)^T\right\} \tag{E.15}$$

$$\mathbf{F}_{\phi\phi} = \frac{2L}{\sigma_n^2}\mathrm{Re}\left\{\left(\dot{\mathbf{\Psi}}^H\mathbf{\Upsilon}^H\mathbf{A}^H\mathbf{A}\mathbf{\Upsilon}\dot{\mathbf{\Psi}}\right)\odot\hat{\mathbf{P}}^T\right\} \tag{E.16}$$

$$\mathbf{F}_{\mathbf{s}_0(i)\mathbf{s}_0(k)} = \frac{2}{\sigma_n^2}\mathrm{Re}\left\{\mathbf{\Pi}^H\mathbf{\Upsilon}^H\mathbf{A}^H\mathbf{A}\mathbf{\Upsilon}\dot{\mathbf{\Psi}}\right\}\delta_{i,k} \tag{E.17}$$

$$\mathbf{F}_{\mathbf{s}_0\mathbf{s}_0} = \mathrm{blkdiag}\left\{\mathbf{F}_{\mathbf{s}_0(1)\mathbf{s}_0(1)}, \mathbf{F}_{\mathbf{s}_0(2)\mathbf{s}_0(2)}, \ldots, \mathbf{F}_{\mathbf{s}_0(L)\mathbf{s}_0(L)}\right\} \tag{E.18}$$

$$\mathbf{F}_{\sigma_n^2\sigma_n^2} = \frac{ML}{\sigma_n^4} \tag{E.19}$$

$$\begin{aligned}\mathbf{F}_{\theta\mu} &= \mathbf{F}_{\mu\theta}^T \\ &= \frac{2L}{\sigma_n^2}\mathrm{Re}\left\{\left(\dot{\mathbf{A}}^H\mathbf{A}_c\right)\odot\left(\mathbf{\Pi}\mathbf{\Psi}_c\hat{\mathbf{P}}_d\mathbf{\Psi}^H\mathbf{\Upsilon}^H\right)^T\right\}\end{aligned} \tag{E.20}$$

$$\begin{aligned}\mathbf{F}_{\theta\nu} &= -\mathbf{F}_{\nu\theta}^T \\ &= -\frac{2L}{\sigma_n^2}\mathrm{Im}\left\{\left(\dot{\mathbf{A}}^H\mathbf{A}_c\right)\odot\left(\mathbf{\Pi}\mathbf{\Psi}_c\hat{\mathbf{P}}_d\mathbf{\Psi}^H\mathbf{\Upsilon}^H\right)^T\right\}\end{aligned} \tag{E.21}$$

$$\begin{aligned}\mathbf{F}_{\theta\phi} &= \mathbf{F}_{\phi\theta}^T \\ &= \frac{2L}{\sigma_n^2}\mathrm{Re}\left\{\left(\dot{\mathbf{A}}^H\mathbf{A}\mathbf{\Upsilon}\dot{\mathbf{\Psi}}\right)\odot\left(\hat{\mathbf{P}}\mathbf{\Psi}^H\mathbf{\Upsilon}^H\right)^T\right\}\end{aligned} \tag{E.22}$$

$$\begin{aligned}\mathbf{F}_{\theta\mathbf{s}_0(i)} &= \mathbf{F}_{\mathbf{s}_0(i)\theta}^T \\ &= \frac{2}{\sigma_n^2}\mathrm{Re}\left\{\mathbf{Q}^H(i)\dot{\mathbf{A}}^H\mathbf{A}\mathbf{\Upsilon}\mathbf{\Psi}\right\}\end{aligned} \tag{E.23}$$

$$\begin{aligned}\mathbf{F}_{\theta\mathbf{s}_0} &= \mathbf{F}_{\mathbf{s}_0\theta}^T \\ &= \left[\ \mathbf{F}_{\theta\mathbf{s}_0(1)}, \mathbf{F}_{\theta\mathbf{s}_0(2)}, \ldots, \mathbf{F}_{\theta\mathbf{s}_0(L)}\ \right]\end{aligned} \tag{E.24}$$

$$\begin{aligned}\mathbf{F}_{\mu\nu} &= -\mathbf{F}_{\nu\mu}^T \\ &= -\frac{2L}{\sigma_n^2}\mathrm{Im}\left\{\left(\mathbf{A}^H\mathbf{A}_c\right)\odot\left(\mathbf{\Pi}\mathbf{\Psi}_c\hat{\mathbf{P}}_c\mathbf{\Psi}_c^H\mathbf{\Pi}^H\right)^T\right\}\end{aligned} \tag{E.25}$$

$$\begin{aligned}\mathbf{F}_{\mu\phi} &= \mathbf{F}_{\phi\mu}^T \\ &= \frac{2L}{\sigma_n^2}\mathrm{Re}\left\{\left(\mathbf{A}_c^H\mathbf{A}\mathbf{\Upsilon}\dot{\mathbf{\Psi}}\right)\odot\left(\hat{\mathbf{P}}_d^H\mathbf{\Psi}_c^H\mathbf{\Pi}^H\right)^T\right\}\end{aligned} \tag{E.26}$$

$$\begin{aligned}\mathbf{F}_{\mu\mathbf{s}_0(i)} &= \mathbf{F}_{\mathbf{s}_0(i)\mu}^T \\ &= \frac{2}{\sigma_n^2}\mathrm{Re}\left\{\mathbf{Q}_c^H(i)\mathbf{A}_c^H\mathbf{A}\mathbf{\Upsilon}\mathbf{\Psi}\right\}\end{aligned} \tag{E.27}$$

$$\begin{aligned}\mathbf{F}_{\mu\mathbf{s}_0} &= \mathbf{F}_{\mathbf{s}_0\mu}^T \\ &= \left[\ \mathbf{F}_{\mu\mathbf{s}_0(1)}, \mathbf{F}_{\mu\mathbf{s}_0(2)}, \ldots, \mathbf{F}_{\mu\mathbf{s}_0(L)}\ \right]\end{aligned} \tag{E.28}$$

$$\begin{aligned}\mathbf{F}_{\nu\phi} &= -\mathbf{F}_{\phi\nu}^T \\ &= \frac{2L}{\sigma_n^2}\mathrm{Im}\left\{\left(\mathbf{A}_c^H\mathbf{A}\mathbf{\Upsilon}\dot{\mathbf{\Psi}}\right)\odot\left(\hat{\mathbf{P}}_d^H\mathbf{\Psi}_c^H\mathbf{\Pi}^H\right)^T\right\}\end{aligned} \tag{E.29}$$

$$\begin{aligned}\mathbf{F}_{\nu\mathbf{s}_0(i)} &= -\mathbf{F}_{\mathbf{s}_0(i)\nu}^T \\ &= \frac{2}{\sigma_n^2}\mathrm{Im}\left\{\mathbf{Q}_c^H(i)\mathbf{A}_c^H\mathbf{A}\mathbf{\Upsilon}\mathbf{\Psi}\right\}\end{aligned} \tag{E.30}$$

$$\begin{aligned}\mathbf{F}_{\nu\mathbf{s}_0} &= -\mathbf{F}_{\mathbf{s}_0\nu}^T \\ &= \left[\ \mathbf{F}_{\nu\mathbf{s}_0(1)}, \mathbf{F}_{\nu\mathbf{s}_0(2)}, \ldots, \mathbf{F}_{\nu\mathbf{s}_0(L)}\ \right]\end{aligned} \tag{E.31}$$

$$\begin{aligned}\mathbf{F}_{\phi\mathbf{s}_0(i)} &= \mathbf{F}_{\mathbf{s}_0(i)\phi}^T \\ &= \frac{2}{\sigma_n^2}\mathrm{Re}\left\{\mathbf{W}^H(i)\dot{\mathbf{\Psi}}^H\mathbf{\Upsilon}^H\mathbf{A}^H\mathbf{A}\mathbf{\Upsilon}\mathbf{\Psi}\right\}\end{aligned} \tag{E.32}$$

$$\begin{aligned}\mathbf{F}_{\phi\mathbf{s}_0} &= \mathbf{F}_{\mathbf{s}_0\phi}^T \\ &= \left[\ \mathbf{F}_{\phi\mathbf{s}_0(1)}, \mathbf{F}_{\phi\mathbf{s}_0(2)}, \ldots, \mathbf{F}_{\phi\mathbf{s}_0(L)}\ \right].\end{aligned} \tag{E.33}$$

As a result, the FIM can be expressed as

$$\mathbf{F} = \begin{bmatrix} \mathbf{F}_{\theta\theta} & \mathbf{F}_{\theta\mu} & \mathbf{F}_{\theta\nu} & \mathbf{F}_{\theta\phi} & \mathbf{F}_{\theta\mathbf{s}_0} & \mathbf{0} \\ \mathbf{F}_{\mu\theta} & \mathbf{F}_{\mu\mu} & \mathbf{F}_{\mu\nu} & \mathbf{F}_{\mu\phi} & \mathbf{F}_{\mu\mathbf{s}_0} & \mathbf{0} \\ \mathbf{F}_{\nu\theta} & \mathbf{F}_{\nu\mu} & \mathbf{F}_{\nu\nu} & \mathbf{F}_{\nu\phi} & \mathbf{F}_{\nu\mathbf{s}_0} & \mathbf{0} \\ \mathbf{F}_{\phi\theta} & \mathbf{F}_{\phi\mu} & \mathbf{F}_{\phi\nu} & \mathbf{F}_{\phi\phi} & \mathbf{F}_{\phi\mathbf{s}_0} & \mathbf{0} \\ \mathbf{F}_{\mathbf{s}_0\theta} & \mathbf{F}_{\mathbf{s}_0\mu} & \mathbf{F}_{\mathbf{s}_0\nu} & \mathbf{F}_{\mathbf{s}_0\phi} & \mathbf{F}_{\mathbf{s}_0\mathbf{s}_0} & \mathbf{0} \\ \mathbf{0} & \mathbf{0} & \mathbf{0} & \mathbf{0} & \mathbf{0} & \mathbf{F}_{\sigma_n^2\sigma_n^2} \end{bmatrix}. \tag{E.34}$$

Consequently, the CRLB can be obtained by taking the inverse of the FIM as

$$\mathrm{CRLB}_{\theta_c} = \sqrt{\frac{1}{N_c}\sum_{i=1}^{N_c}[\mathbf{F}^{-1}]_{ii}} \tag{E.35}$$

$$\mathrm{CRLB}_{\theta_u} = \sqrt{\frac{1}{N_u}\sum_{i=N_c+1}^{N}[\mathbf{F}^{-1}]_{ii}} \tag{E.36}$$

$$\mathrm{CRLB}_{\phi_u} = \sqrt{\frac{1}{N_u}\sum_{i=N+2N_c+1}^{N+2N_c+N_u}[\mathbf{F}^{-1}]_{ii}}. \tag{E.37}$$

References

[1] P. Chargé, Y. Wang, J. Saillard, A non-circular sources direction finding method using polynomial rooting, Signal Process. 81 (8) (2001) 1765–1770.

[2] M. Haardt, F. Roemer, Enhancements of unitary ESPRIT for noncircular sources, Montreal, QC, Canada, in: Proceedings of the IEEE International Conference Acoustic, Speech and Signal Process. (ICASSP), 2, 2004, pp. 101–104.

[3] J. Steinwandt, F. Roemer, M. Haardt, G.D. Galdo, *R*-Dimensional ESPRIT-type algorithms for strictly second-order non-circular sources and their performance analysis, IEEE Trans. Signal Process. 62 (18) (2014) 4824–4838.

[4] H. Abeida, J.P. Delmas, MUSIC-like estimation of direction of arrival for noncircular sources, IEEE Trans. Signal Process. 54 (7) (2006) 2678–2690.

[5] J. Liu, Z. Huang, Y. Zhou, Extended 2*q*-MUSIC algorithm for noncircular signals, Signal Process. 88 (6) (2008) 1327–1339.

[6] F. Gao, A. Nallanathan, Y. Wang, Improved MUSIC under the coexistence of both circular and noncircular sources, IEEE Trans. Signal Process. 56 (7) (2008) 3033–3038.

[7] H. Chen, C. Hou, W. Liu, W.-P. Zhu, M.N.S. Swamy, Efficient two-dimensional direction-of-arrival estimation for a mixture of circular and noncircular sources, IEEE Sens. J. 16 (8) (2016) 2527–2536.

[8] J.P. Delmas, H. Abeida, Stochastic Cramér–Rao bound for noncircular signals with application to DOA estimation, IEEE Trans. Signal Process. 52 (11) (2004) 3192–3199.

[9] F. Roemer, M. Haardt, Deterministic Cramér–Rao bounds for strict sense non–circular sources, Vienna, Austria, in: Proceedings of the ITG/IEEE Workshop Smart Antennas (WSA), 2007.

[10] H. Abeida, J.P. Delmas, Statistical performance of MUSIC-like algorithms in resolving noncircular sources, IEEE Trans. Signal Process. 56 (9) (2008) 4317–4329.

[11] T.J. Shan, T. Kailath, Adaptive beamforming for coherent signals and interference, IEEE Trans. Acoust. Speech Signal Process. 33 (3) (1985) 527–536.

[12] T.J. Shan, M. Wax, T. Kailath, On spatial smoothing for direction-of-arrival estimation of coherent signals, IEEE Trans. Acoust. Speech Signal Process. 33 (4) (1985) 806–811.

[13] J.A. Cadzow, Y.S. Kim, D.C. Shiue, General direction-of-arrival estimation: a signal subspace approach, IEEE Trans. Aerosp. Electron. Syst. 25 (1) (1989) 31–47.

[14] D.A. Linebarger, R.D. DeGroat, E.M. Dowling, Efficient direction-finding methods employing forward/backward averaging, IEEE Trans. Signal Process. 42 (8) (1994) 2136–2145.

[15] F.M. Han, X.D. Zhang, An ESPRIT-like algorithm for coherent DOA estimation, IEEE Antennas Wirel. Propag. Lett. 4 (1) (2005) 443–446.
[16] S.U. Pillai, B.H. Kwon, Forward/backward spatial smoothing techniques for coherent signal identification, IEEE Trans. Acoust. Speech Signal Process. 37 (1) (1989) 8–15.
[17] R. Rajagopal, P.R. Rao, Generalized algorithm for DOA estimation in a passive sonar, IEE Proc. F Radar Signal Process. 140 (1) (1993) 12–20.
[18] J.S. Thompson, P.M. Grant, B. Mulgrew, P. Rajagopal, Generalized algorithm for DOA estimation in a passive sonar, IEE Proc. F Radar Signal Process. 140 (5) (1993) 339–340.
[19] C. Qi, Y. Wang, Y. Zhang, Y. Han, Spatial difference smoothing for DOA estimation of coherent signals, IEEE Signal Process. Lett. 12 (11) (2005) 800–802.
[20] Z. Ye, X. Xu, DOA estimation by exploiting the symmetric configuration of uniform linear array, IEEE Trans. Antennas Propag. 55 (12) (2007) 3716–3720.
[21] Z. Ye, Y. Zhang, X. Xu, C. Liu, Direction of arrival estimation for uncorrelated and coherent signals with uniform linear array, IET Radar Sonar Navig. 3 (4) (2009) 144–154.
[22] F. Liu, J. Wang, C. Sun, R. Du, Spatial differencing method for DOA estimation under the coexistence of both uncorrelated and coherent signals, IEEE Trans. Antennas Propag. 60 (4) (2012) 2052–2062.
[23] Y. Wang, M. Trinkle, B.W.-H. Brian, Two-stage DOA estimation of independent and coherent signals in spatially coloured noise, Signal Process. 128 (2016) 350–359.
[24] P. Stoica, A. Nehorai, MUSIC, maximum likelihood, and Cramer–Rao bound, IEEE Trans. Acoust. Speech Signal Process. 37 (5) (1989) 720–741.
[25] A.J. Weiss, B. Friedlander, On the Cramér–Rao bound for direction finding of correlated sources, IEEE Trans. Signal Process. 41 (1993) 495–499.
[26] P.J. Schreier, L.L. Scharf, Statistical Signal Processing of Complex-Valued Data: The Theory of Improper and Noncircular Signals, Cambridge University Press, Cambridge, U.K., 2010.
[27] M. Pesavento, A.B. Gershman, K.M. Wong, Direction finding in partly-calibrated sensor arrays composed of multiple subarrays, IEEE Trans. Signal Process. 50 (9) (2002) 2103–2115.
[28] C.M.S. See, A.B. Gershman, Direction-of-arrival estimation in partly calibrated subarray-based sensor arrays, IEEE Trans. Signal Process. 52 (2) (2004) 329–338.
[29] R.O. Schmidt, Multiple emitter location and signal parameter estimation, IEEE Trans. Antennas Propag. 34 (3) (1986) 276–280.
[30] R. Roy, T. Kailath, ESPRIT-estimation of signal parameters via rotational invariance techniques, IEEE Trans. Acoust. Speech Signal Process. 37 (7) (1989) 984–995.
[31] H. Yan, H.H. Fan, On source association of DOA estimation under multipath propagation, IEEE Signal Process. Lett. 12 (10) (2005) 717–720.